CHALMERS
UNIVERSITY OF TECHNOLOGY

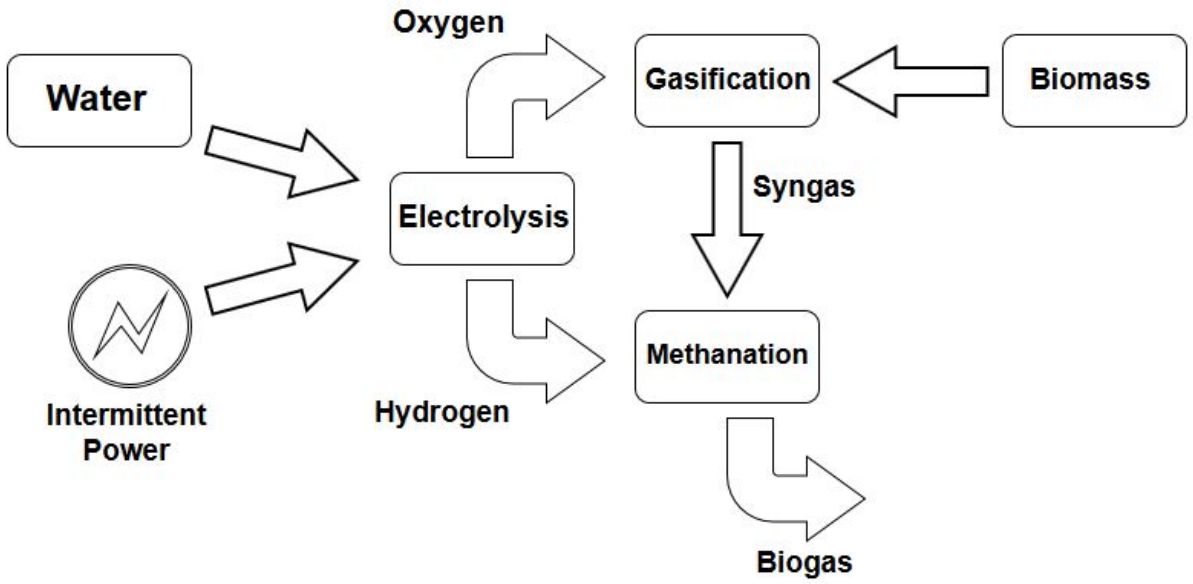

Power-to-Gas concepts integrated with syngas production through gasification of forest residues

Process modelling

Master's thesis in Sustainable Energy System Programme

Andrea Gambardella & Yahya Yasin Yahya

Department of Energy and Environment
CHALMERS UNIVERSITY OF TECHNOLOGY
Göteborg, Sweden 2017

Master's thesis 2017

Power-to-Gas concepts integrated with syngas production through gasification of forest residues

Process modeling

Andrea Gambardella & Yahya Yasin Yahya

CHALMERS
UNIVERSITY OF TECHNOLOGY

Department of Energy and Environment
Division of Energy Technology
Chalmers University of Technology
Göteborg, Sweden 2017

Power-to-Gas concepts integrated with syngas production through gasification of forest residues
Process modelling

Master's Thesis within the Sustainable Energy System
Andrea Gambardella & Yahya Yasin Yahya

Supervisor: Johan Ahlström, Department of Energy and Environment
Examiner: Stavros Papadokonstantakis, Department of Energy and Environment

Master's Thesis 2017
Department of Energy and Environment
Division of Energy Technology
Chalmers University of Technology
SE-412 96 Göteborg
Telephone +46 31 772 1000

Cover: Gasification of biomass with integrated power-to-gas concept.

Chalmers Reproservice Göteborg, Sweden 2017

Power-to-Gas concepts integrated with syngas production through gasification of forest residues
Process modelling

Master's Thesis within the Sustainable Energy System
Andrea Gambardella & Yahya Yasin Yahya
Department of Energy and Environment
Division of Energy Technology
Chalmers University of Technology

Abstract

Climate change and global warming caused by the emission of CO_2 from fossil fuels utilization are one of the most challenging environmental threat mankind is facing nowadays. As motives to reduce CO_2 emissions, the attentions to replace the fossil fuels with renewable energy sources such as biomass, sun and wind is high on agenda in the recent decades. However, these renewable resource suffer from some drawbacks: the intermittent nature of the electricity from the sun and the wind destabilize the electric grid and energy from biomass is not easily accessible to be used in the transport sector for example, which is the major CO_2 emitter. By a thermo-chemical process called gasification, biomass can be reacted to produce syngas (mixture of CO_2 CO, H_2, CH_4) which can be used to synthesize secondary bio-fuels such as biogas, methanol and Fischer-Tropsch. Through power-to-gas technology the intermittent electricity can be used in the gasification system. Gasification and Power-to-gas technology together can work in synergy enhancing the production of secondary biofuels, while increasing the integration of intermittent energy sources in the energy system and even stabilizing the electric grid.

This project is concerned with the modeling of biomass gasification in a pressurized, oxygen-blown, fluidized bed gasifier and integration of power-to-gas technology in the gasification system. The model is based on experimental data available in a literature and developed by flowsheeting in ASPEN PLUS. The model includes processes such as biomass drying, biomass gasification, methanation of the syngas and the Sabatier process. Four different layouts of the Sabatier process are developed to investigate and compare the thermodynamic performance (energy and exergy efficiency), economic performance (operational profits) and operational flexibility of layouts when integrating power-to-gas concept in the gasification system. The layout upstream of the Sabatier reactor is identical for every scenario and it has a CH_4 yield of $0,24 \mathrm{kg}_{\mathrm{CH_4}}/\mathrm{kg}_{\mathrm{drybiomass}}$. An important aspects of the different layouts is in the CO_2 removal unit position and utilization: the CO_2 can be fed to the Sabatier reactor either mixed in the gas coming from the methanation unit, or pure. In the former case all the CO_2 is injected but only the unreacted has to be separated at the end of the process, whereas in the latter almost all the CO_2 is removed, but then only the desired amount is injected into the reactor. Energy and exergy efficiencyof the system is in the range of 0,55 - 0,8 and 0,35 - 0,4 respectively, while the operational revenues can peak $0,22 \mathrm{USD}/\mathrm{kWh}_{\mathrm{drybiomass}}$. Concerning the operational

performances (economic, thermodynamic and flexibility) it was noticed that feeding the Sabatier reactor with the entire mix of gases coming from the methanation unit, and separating the unreacted CO_2 afterwards was the most advantageous scenario, but it may lead to higher investment cost.

Keywords: gasification, biomass, gasifier, product gas, biomethane, power-to-gas, Sabatier reactor, biogas, ASPEN PLUS, methanation,

Acknowledgements

Our sincere gratitude goes to Stavros Papadokonstantakis and Johan Ahlström who patiently guided us throughout the progression of this work.

Andrea Gambardella & Yahya Yasin Yahya, Gothenburg, May 2017

Contents

List of Figures

List of Tables

1
Introduction

One of the most challenging problems that humanity is facing today is climate change, which is manifesting itself in the form of global warming and unusual weather patterns such as floods and storms. The main cause of the climate change is the emission of CO_2 (greenhouse gas) from the fossil fuels which is the main energy source of the world. In order to slow down the climate change, it is important to consider the reduction of fossil fuel use and its eventual replacement by renewable and environmentally friendly energy sources. Biomass is one of the energy sources considered to be a viable and alternative to the fossil fuels.

By a thermochemical process called gasification, biomass can be reacted into useful product gas. The product gas (the syngas) is a mixture of CO, H_2, CH_4, CO_2, light hydrocarbons (ethane and propane) and heavier hydrocarbons such as tars [1]. The product gas from biomass can be used in the production of useful chemicals and second-generation biofuels such as biomethane, methanol, Fischer-Tropsch liquids and hydrogen. These biofuels can be used both in the transport sector (for example for natural-gas driven vehicles), and in heat and power production plants thereby paving the way for the implementation of renewable energy in the energy system [2][3][4].

The motive to increase the share of renewable energy in the energy system is leading to the rise in production of electricity from energy sources such as wind and sun. However, the electric power generated by these sources destabilize the grid due to their intermittent nature. Therefore, it would be advantageous to develop a mechanism which helps utilize the full potential of intermittent energy sources while maintaining the stability of the electric grid at the same time. Power-to-gas (P2G) technology together with the gasification might be the promising system for that purpose. Indeed, P2G (like water electrolysis) is already considered as an option to stabilize the electric grid by smoothing out load peaks due to unpredicted power generation, furthermore this technology can work in synergy with gasification to enhance biogas production (as it will be shown later on in the report) for an even better energy recovery.

There are two types of gasification technologies: autothermal (direct) and allothermal (indirect) gasification. In the former technology the heat required by the process is only internally generated by the partial combustion of the feedstock, whereas in the latter technology energy is delivered to the process also through the gasifying agent (steam). Furthermore, in the direct gasification, all the reactions occur in the

same device, while in the indirect, combustion reactions occur in a separate chamber, which communicates with each other both with mass streams (bed material, char, ashes and feedstock to be combusted) and energy streams (heat carried by the thermal inertia of the bed material itself). Figure 1.1 shows the direct and indirect gasification system [5].

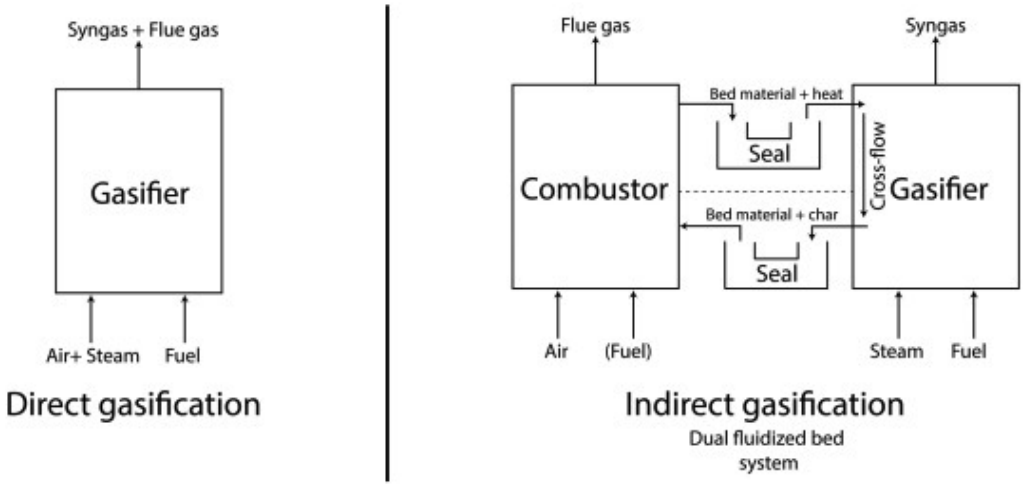

Figure 1.1: Direct and indirect gasification reactor [5].

In the indirect gasifier, the flue gases of the combustion (mainly H_2O, CO_2 and N_2) do not mix with the product gas because the oxygen carrier to the gasifier is the oxidized recirculating bed material. However, in the direct gasifier, the flue gases are mixed into the products and combustion occurs only partially (lambda < 1) [3][6]. Be authothermal or allothermal, the most known type of reactors used for the gasification process are moving-bed, fluidized bed(reactor temperature of 800-1000°) and entrained flow reactor (reactor temperature over 1000°) [2].

In a previous study [7], an indirect gasification plant of 100MW thermal power was simulated in ASPEN PLUS. In the simulation, biomass (forest residues) was gasified in order to produce biomethane. It is, therefore, of interest to simulate a direct gasification plant of biomass and analyze the integration of power-to-gas (P2G) technology to the gasification system, and thereby compare the performance of the two gasification technologies. Table 1.1 shows the two types of biogas with the corresponding specifications according to Swedish standard.

Table 1.1: Properties of Biogas type A and B according to Swedish standard SS 15 54 38 [8].

Properties	Type A	Type B
Wobbeindex (MJ/m^3)	44,7 – 46,4	43,9 – 47,3
CH_4 content (vol-%)	97 ± 1	97 ± 2
Water content (mg/Nm^3)	32	32
O_2 content (max, vol-%)	1,0	1,0
$CO_2 + N_2 + O_2$ (vol-%)	4,0	5,0
Sulfur contaminants (mg/Nm^3)	23	23
NH_3 (mg/Nm^3)	20	20

1.1 Objectives

In this project, the assessment of power-to-gas technology (P2G) integrated with direct gasification plant is carried out through modeling in ASPEN PLUS. The main product of the plant is biomethane, but other valuable products such as steam from process heat, surplus oxygen and electricity generation have been considered for the plant economic and energy performance also. Pure oxygen has been considered as gasification agent, while hydrogen is injected to the Sabatier reactor to enhance the CH_4 yield of the process while simultaneously decreasing the CO_2 emissions. The main goals of the projects are:

- to develop a plant layout, through ASPEN PLUS, which resembles reality both at system and process level [1]
- to develop different layouts for power to gas integration.
- to assess the economic (operational profits) and energy performances of the plant and its power to gas integration scenarios.

The above mentioned goals will be fulfilled by:

- creating a framework in Excel where result data from ASPEN PLUS can easily be retrieved.
- generating Matlab code which can use the Excel framework to perform heat integration and assess the performance of the model.

1.2 Scope of the project

What fall outside the project objectives is the economic evaluation of the plant size, investment costs, logistic etc. Nevertheless, concepts concerning the size variation of the plant units for different scenarios will be provided as a base for future studies. The environmental impact of the plant is also not assessed. The plant performances are assessed under steady state conditions, both energy and material wise, while no fluid or process dynamics have been investigated. Sensitivity analysis have been conducted by varying hydrogen and carbon dioxide feed into the Sabatier reactor simultaneously, all the parameters affected by this streams (such as reactor size or

[1] The model is based on the experimental data produced by Hannula et al [9] by gasifying forest residues in an oxygen-blown fluidized bed gasifier.

catalyst load) are varied accordingly, whereas all the non affected parameters are kept constant. The experimental data acquired from Hannula et al. [9] is produced from the direct gasification forest residues (lignocellulosic), and the produced biogas quality is evaluated on its chemical composition and categorized as type A or B according to the Swedish standard [8] for the biogas. Regarding the environmental condition that could affect the performance, the plant is supposed to be located close to the city of Göteborg in Sweden.

2
Theory

2.1 Gasification of biomass

Generally, the gasification process of biomass undergoes the following steps: drying, pyrolysis (thermal decomposition), partial combustion, and gasification of volatile products. Figure 2.1 depicts a typical biomass gasification process [2]. The sequence of gasification reactions depend up on the type of reactor used such as moving-bed reactor, fluidized-bed reactor and entrained-flow reactor, see Figure 2.2 for the sequence of gasification process in a moving-bed reactor [2].

The gasifying agent is a medium used to gasify the feedstock and it can either be air, pure O_2, steam or a mixture of them. However, using air as a gasifying agent in autothermal gasification results in a product gas rich in N_2 (and therefore results in low heating value). Studies have shown that a pressurized oxygen-blown autothermal gasifier outperforms an indirect gasifier economically, thermodynamically and exergetically [4]. Furthermore, an authothermal system is simpler and easier to operate. Neverthless, the allothermal gasifier can produce a N_2-free product gas (because air is not used as gasifying agent) and the system reaches a complete carbon conversion without production of problematic waste products [6].

The quality of a product gas produced is determined by properties such as H_2/CO ratio, amount of inerts in the product gas, amount of methane and amount of poisonous agent such as sulfur- and chlorine component. The content of sulfur and chlorine impurities depends on the type of feedstock used in the gasification [6]. The H_2 content in the product gas for indirect gasification is higher than that of direct gasification. However, the content of CO is to the contrary [1]. The H_2/CO of the product gas is therefore has to be adjusted in order to get the required synthesis ratio, which normally is between 1,5 and 3 for the synthesis of biomethane. The ratio adjustment can be done by water-gas-shift reaction in a separate catalytic reactor [6].

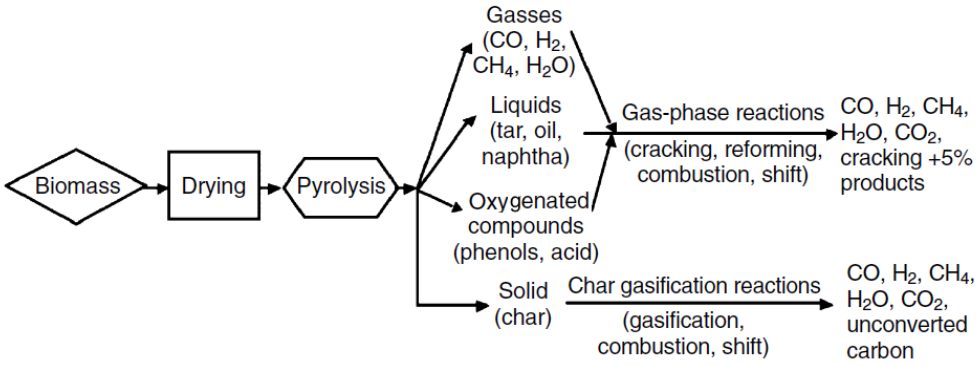

Figure 2.1: Path of a gasification process [2].

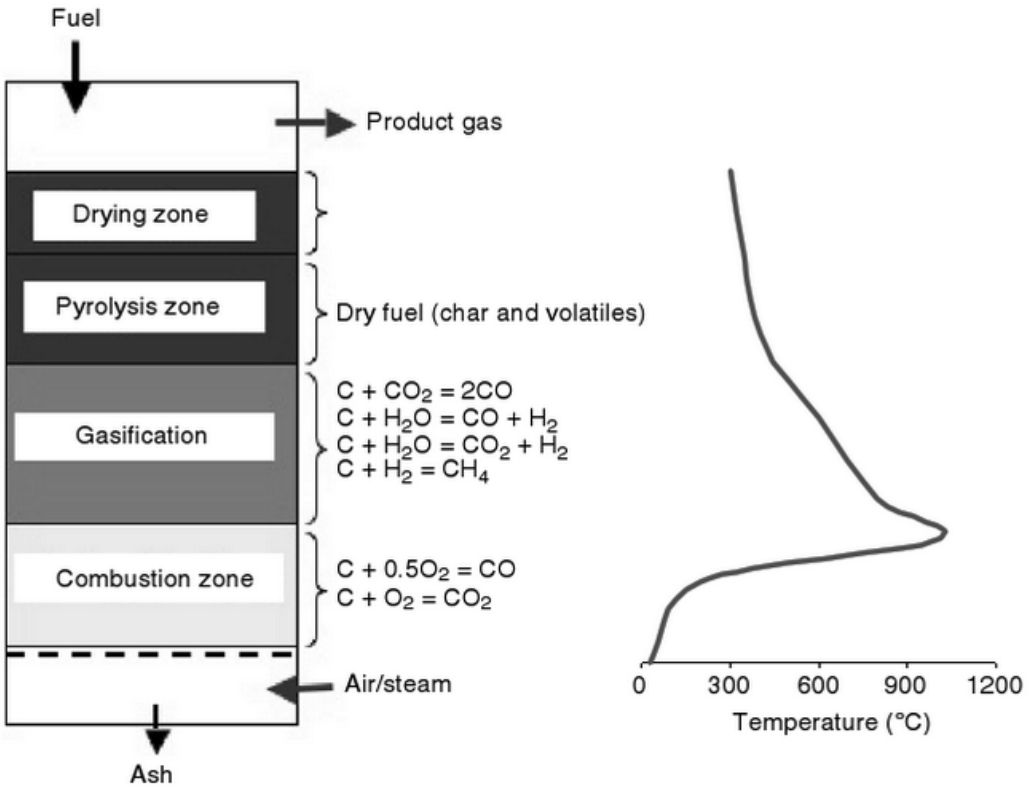

Figure 2.2: The gasification sequence and temperature level in a typical moving bed-reactor gasifier [2].

2.1.1 Drying of biomass

One major difference between a conventional fuel such as coal and biomass is that the later has significantly higher content of moisture, with 50-60% wet basis (w.b) of moisture in the woody biomass. Fuel drying helps to sustain the gasification and decreases the need of auxiliary fuel. Additionally, drying biomass prior to gasification is beneficial because it reduces the size of the gasifier and the feeding system required. Usually, the biomass moisture prior to feeding the biomass into the gasifier

is reduced below 15% w.b [10].

Definition for the heat required in the drying process varies. Usually it is defined to be the heat required to evaporate the moisture of the biomass, while the rising of the moisture's temperature to the saturation is also accounted for in some other cases [11]. In these definitions, the energy required to extract the water molecules bonded to the cellular structure of the biomass is not considered. The consideration to this energy requirement necessitate the development and usage of an empirical formula or the usage of advanced computer simulation such as Computational Fluid Dynamics (CFD) which helps determine the needed energy.

For a typical biomass with Lower Heating Value (LHV) of 19 MJ/kg and moisture content of 50% w.b, the energy required to completely evaporate the moisture and heat the biomass up to the gasifier temperature of 900° is around 22% of the LHV. However, if the biomass, for example, is dried to 10% w.b prior to gasification, the energy demand can be reduced to 2,5% [10]. Therefore, it is advantageous from the energy point of view to integrate the drying system with the gasification system so that the waste heat at lower temperature is used. The heat required in the drying process can be internally recovered and is supplied with the drying agents (examples of drying agents are: steam, hot air, or hot flue gases)[10][11]. Heyne et al. [11] investigated the integration of drying system where steam, flue gas and air is used as drying agent with an indirect gasification plant of 100 MW_{th}. It was shown that steam drying performs better, covering around 50% of the energy demand to dry biomass from 50% w.b to 10% w.b [11]. In the drying process, precaution has to be taken as there could be a risk of explosion and fire, specially in the case of air drying, due to the collection of volatile organic compounds [10].

The most common types of dryer used for biomass drying are fluidized bed dryers, rotary dryers, super-heated steam dryers and belt dryers. Alamia et al. [10] proposes the belt dryer for gasification process because of low fire risk, high exploitation of low temperature heat (below 130°), and thereby offers chances of heat recovery. In a belt dryer, biomass with a bed thickness of 2-30 cm is conveyed over a porous belt whereby the drying medium is blown from the bottom by fans through the belt. Figure 2.3 illustrates a two staged belt dryer where air at 100° (or below) is used to dry the biomass from 50% w.b to 10-20% w.b in the first stage, and steam with temperature of 120-150° is used in the second stage [10].

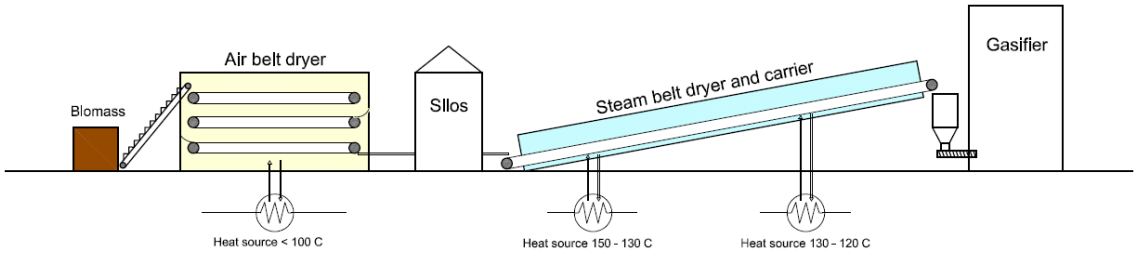

Figure 2.3: The belt dryer as proposed by Alamia [10].

2.1.2 Pyrolysis

Pyrolysis is a process which occurs also in gasification. In the pyrolysis step the feedstock (biomass) is thermally degraded in absence, or low presence of oxygen to produce various gas components such as H_2, CO, CO_2, H_2O, C_2H_2, C_2H6, C_6H_6, tar and solid char [2]. During pyrolysis, 70-80% of the biomass weight is devolatalized at the temperature of around 500° [12].

Tar is a complex organic product that consists predominantly of different types of aromatic hydrocarbons. The formation and composition of tar during gasification process depends on conditions such as operation temperature and the feedstock [13]. In the temperature range of 400-700°, biomass gives rise to the so called primary tar which constitutes oxygenated organic molecules such as acetic acid, hydroxypropanone and methanol, and aromatic compounds such as toluene and benzene. For steam gasification at higher temperature (900-1000°), tar consists aromatic hydrocarbons such as benzene, toluene and naphthalene [14].

2.1.3 Char gasification and combustion

The pyrolysis step is followed by the step where chemical reactions between the volatile matters such as steam, hydrocarbons, carbon dioxide, hydrogen and char gasification take place. The char of biomass contains primarily carbon (85%) and a little inorganic ashes with oxygen and hydrogen. The biomass char is more reactive than the coke (char of coal), owing to alkali metals which work as catalysts. The possible reaction that arises during the gasification of char are described as follows [2]

$$\text{Char} + O_2 \longrightarrow CO_2/CO \tag{2.1}$$

$$\text{Char} + CO_2 \longrightarrow CO \tag{2.2}$$

$$\text{Char} + H_2O \longrightarrow CH_4 + CO \tag{2.3}$$

$$\text{Char} + H_2 \longrightarrow CH_4 \tag{2.4}$$

Both exothermic and endothermic reactions occur during gasification. Therefore, it is important for the process in order to be autothermal (heat self-sustained) that the energy released by the exothermic reaction is sufficient to satisfy the energy needs of the endothermic ones. Reaction 2.1 is the most exothermic reaction of the gasification process which bestows 394 kJ/mol and 111 kJ/mol of heat energy depending on if CO_2 and CO produced respectively [2].

2.1.4 Oxygen for direct gasification

Of the gasifying agents (oxygen, steam and air) oxygen is the best medium in generating a product gas with high heating value (12-28 MJ/Nm^3). Moreover, the use of pure oxygen as gasifying medium shrinks the size of reactor and auxiliary systems recommended [2]. Nevertheless, pure oxygen has to be generated, bringing energetic/economic penalty on the the system. Commercially, oxygen is produced through

separating air into its components; mainly nitrogen and oxygen. The most common technologies used for air separation are cryogenic air separation (ASU), membrane and pressure swing adsorption (PSA). In ASU technology, air is cooled down until it liquefies, and the components of the air are then selectively separated based on their boiling points. Even though ASU is an energy intensive process, it is the most widely used technology for the voluminous production of oxygen with high purity [15]. Table 2.1 shows the comparison of energy performance for different types of air separation units [16].

Table 2.1: Comparison of different air separation technologies [16].

Technology	O_2 purity	Capacity (ton/day)	Energy demand kWh/ton O_2	Driving force
Cryogenic	99+	up to 4000	200	Electricity
PSA	95+	up to 300	245 [4]	Electricity Heat (70-90°C)
Membrane (polymer)	99+	up to 20	—	Electricity

2.2 Gas treatment

The product gas leaving the gasifier is a mixture of CO, CO_2, H_2, CH_4, H_2O, inorganic impurities (H_2S, HCl etc), and organic compounds such as tars, aliphatic hydrocarbons, toluene and benzene (if the gasification process is operated below 1000°C). The produced gas has to be, therefore, purified of impurities and treated in the downstream process in order to meet the specification of the end-product, biomethane in this case. Additionally, the cleaning and upgrading systems employed for these purposes have to be efficient and economically feasible. [1].

2.2.1 Gas purification

The product gas has to be purified from catalyst poisoning impurities in order to decrease downstream process maintenance costs. The most known impurities in the product gas from direct gasification of biomass are particulate matter, volatile metal oxides (NaCl and KCl), tars and sulfur compounds (H_2S and COS). The removal of these impurities in the downstream process takes place according to the presented order [1].

2.2.2 Particulate matter

Particulate matter in the product gas consists of ash particles, unreacted carbon, soot (in the case of direct gasification) and particles of bed materials when fluidized bed gasifier is used for gasification. Technologies used to remove particulate matter from the product gas are cyclones, filters (electrostatic and barrier) and scrubbers. The volatile metal oxides in the product gas is also removed when removing particulate matter with the application of filters and scrubbers. Table 2.2 shows different

technologies for removing particulate matter with their efficiency and operation temperature [1].

Table 2.2: Particle separators with their performance and operation temperature [1].

Technology	Temperature(degC)	Particle reduction (%)
Cyclone	20-900	45-70
Sandbed filter	20-900	80-95
Bag filter	150-750	90-99
Scrubber	20-200	40-65
Electrostatic precipitator	40-50	95-99

2.2.3 Tar destruction

The existence of tar in the gas product is undesirable as tar may condense on the surface of heat exchangers and block gas cleaning filter in the downstream process, leading to operational problems. Therefore it is necessary to remove or destroy the tar. Tar of the product gas at 400-900°C is catalytically disintegrated into CO and H_2 with the help of nickel-based catalyst. The main disadvantage of this method is that inorganic impurities in the product gas may impair the performance of the catalyst. Therefore, these impurities have to be cleaned off by particulate separators prior to catalytical destruction of the tar. In a direct gasification with an entrained flow gasifier, tar can be thermally cracked at high temperature (over 1000°C) [1] [14].

The most promising method of scrubbing tar from the product gas is the so called physical scrubbing, where organic liquids such as biodiesel is used to wash away the tar from the product gas [1]. This method is employed at GoBiGas where rape methyl ester (RME) of 0,03-0,035 $MW_{RME}/MW_{biomass}$ amount is used to scrub the tar from the product gas. The RME together with the captured tar is recirculated to the combuster to be burned [7].

2.2.4 Sulfur contaminants

Generally, the percentage amount of sulfur in biomass feedstock is low: ranging from 0,3-0,4% (w/w) in herbaceous biomass to <0,1% in woody biomass. Sulfur in the biomass feedstock is converted during gasification to H_2S, COS or sulfur oxides(SO_x), depending on the type of gasification used. The low concentration of sulfur in the biomass does not entail the removal of sulfur contaminants when the biomass product is used as fuel for example. However, when the product gas of the biomass is used for synthesis, the removal of sulfur contaminants is mandatory because these contaminants jeopardize the performance of catalysts in the downstream. H_2S is the major sulfur contaminants which is harmful and corrosive and has to be removed from the product gas of gasification. Not all the H_2S can be removed (due to the efficiency of the removal unit), nevertheless the acceptable H_2S

content in the produced biomethane has to be kept below 1 ppm [17].

There are a number of methods used for the removal of H_2S from the product gas. The method is chosen based upon the specification of the intended product, the characteristics of the gas composition and amount of gas to be treated. The method used to remove H_2S can be biological or chemical-physical, where chemical and physical solvents are jointly used to remove H_2S [1]. Absorption with chemical solvents is favourable when the partial pressure of the acidic gases (H_2S, CO_2) is low, while the usage of physical solvents perform better at higher partial pressure [1].

The removal of acidic gases from a gas stream is conventionally done at lower temperature (20-25°C) by gas-liquid absorption process where aqueous solutions of amines such as MEA (monoethanolamine), DEA (diethanolamine) and MDEA (methyldiethanolamine) are used, (this process is similar to the CO_2 capture, see Figure 2.5). The advantage of using alkanolamines for the removal of acidic gases is that it can be used in such a way so that the absorption of the desired gas is favoured [18][1]. For exemple, non-aqueous MDEA reacts only with H_2S, however, as the water content of MDEA solution increases, the co-absorption of CO_2 also increases, leading to the decrease in the selectivity of H_2S as it is shown in the experiment done by Hong et al. [19]. According to the experiment done by Zhi et al. [20], the optimal MDEA concentration for the best selectivity and efficiency for removing H_2S is 20% (w/w). They have experimentally demonstrated that one can, when using 15% (w/w) aqueous MDEA solution at operation temperature of 40°C, achieve a 98.7% of H_2S removal from a gas stream. In such process, 9,50% of CO_2 in the gas stream is co-absorbed [20].

The regeneration energy required when using MDEA as solvent is less than that of MEA, which is 2,4 kg of saturated steam (at temperature of 100-150°C [21]) per kg of H_2S eliminated. The absorption capacity of MDEA is around 0,7-0,8 moleH_2S/moleMDEA [22]. MDEA reacts with H_2S according to reaction 2.5 [1].

$$R3-N + H2S \longleftrightarrow R3NH^+ + HS^- \tag{2.5}$$

When using MDEA to remove H_2S, the absorber and desober function at high pressure (7-70 bar) and atmospheric pressure respectively, and the operation temperature of lower than 60°C is recommended for an adequate absorption. The main benefit of using amines for the scrubbing of H_2S, in comparison to CO_2 scrubbing, is that the rate of reaction between amines and H_2S is faster, the heat transfer coefficient is also higher. This enables the usage of a relatively smaller absorption unit [1].

Generally, using amines in the gas-liquid absorption process is considered energy intensive, and amines are caustic and degradable. Studies are ongoing in order to develop a superior, energy efficient and economically feasible solid sorbent which can remove H_2S from a gas stream at higher temperature (>300°C). Various metal oxides such as ZnO, CaO, Al_2O_3 and MgO, and compounds such as zeolites are being tested and studied [18].

2.3 Water-gas-shift for the syngas

The most important components of syngas are H_2 and CO. The composition ratio (H_2/CO) of these two gases has to be adjusted depending on the types of the chemicals to be synthesized in the downstream process, and for the production of biomethane this ratio is between 1,5 and 3. The H_2/ CO ratio of the product gas can be adjusted by the water-gas-shift:

$$CO + H_2O \longleftrightarrow CO_2 + H_2 \qquad \Delta H = -41{,}2\,\mathrm{kJ/mol} \tag{2.6}$$

The equilibrium of reaction 2.6 in the mixture of the product gas depends on the temperature, not on the pressure (if the pressure is below 70 bar). Without a catalyst the equilibrium of the reaction is instantaneously reached at a temperature above 950°C. With the presence of catalyst temperature can be lowered, and two temperature ranges are used for the water-gas-shift reaction at industrial level: 300-510°C (copper catalysts) and 180-270°C (aluminium oxide-copper-zinc catalysts) [1].

2.4 Methanation of the syngas

The need for the production of synthetic natural gas (SNG) from biomass is high because of the surging price of natural gas and the will to reduce the reliance on natural gas. At the core of producing SNG is the methanation process where the dry and purified syngas is converted to methane according to reaction 2.7 [23][24].

$$CO + 3\,H_2 \longrightarrow CH_4 + H_2O \qquad \Delta\,\overset{\circ}{H} = -206{,}2\,\mathrm{kJ/mol} \tag{2.7}$$

CO_2, which is present in the syngas, can also react with H_2 according to the Sabatier reaction (reaction 2.8) to form methane. However, in a gas mixture that contain CO, the methanation of CO, reaction 2.7, is more favoured. The (exothermic) heat released during the reaction favours the reverse water-gas-shift (reaction 2.6), thereby increasing CO concentration, and suppresses CO_2 methanation [25]. Therefore the methanation of syngas, unlike that of CO_2, can be operated at higher temperature.

Two types of reactors are used for the methanation process: fixed and fluidized bed [23][24]. Companies such as Kernforschungszentrum Jülich (Germany), Haldor Topsøe (Denmark) [26] and Sasolburg (South Africa) have, since the 1970s, extensively worked on the development of methanation reactors at both demonstration and pilot scales. They have conducted methanation in a seriously connected adiabatic fixed bed reactors. The operation temperature and pressure in reactors are 250-700°C and up to 30 bar, respectively. The temperature of the gas stream in such system is controlled by inter-cooling or recycling of the product gas, see Figure 2.4 [23]. The research and studies done by these companies culminated in the development of the first and only commercial methanation plant which was commissioned in 1984 in Dakota USA. The plant is operated by Dakota Gasification Company and can produce 4,8 million m^3 of SNG per day [27].

An other methanation reactor built, as a demonsntartion plant, is that of the Gobi-Gas (Gothenburg Biomass Gasification Project) plant. The constraction of GoBiGas was started in 2011 and completed in november 2013. This plant is the first of its kind where biomass is gasified and converted into biomethane. Currently, the plant has the capacity of $32\text{MW}_{\text{biomass}}$, and there is a plan to develop the plant into a commercial level with a capacity of $100\text{MW}_{\text{biomass}}$.

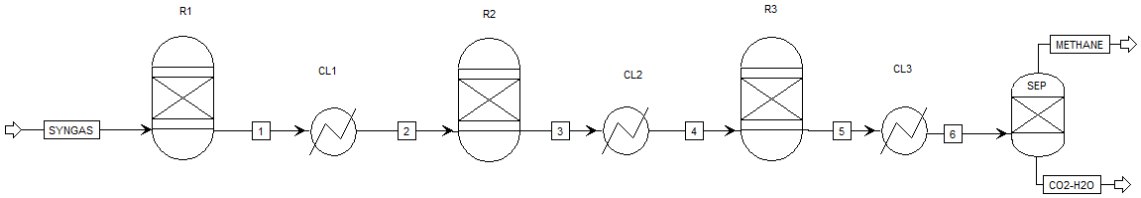

Figure 2.4: Configuration of methanation reactor. Acronyms are: R_i is reactors; Cl_i is cooler; SEP is the flash separator.

The usage of fluidized bed reactors for the methanation process is advantageous for large scale operation when the involved reactions of the methanation has to be heterogeneously catalyzed. The turbulence condition in the fluidized bed offer, in comparison to the fixed bed, higher heat transfer coefficient, thereby facilitating a better temperature control, an isothermal operation and requirement of fewer reactors [28]. Additionally, the continuous removal and addition of catalysts are possible in the case of fluidized bed. However, care has to be taken when using fluidized bed as catalysts may entrained. In the fixed bed reactor, the problem related with catalysts is sintering due to high temperature in the reactor. Thermodynamically, the methanation process is favoured at low temperature and high pressure [23].

Different types of catalysts are used for the methanation of the syngas in fixed bed and fluid bed. The catalysts for the methanation in fixed bed are commercially available, however, there is no catalyst ready to be used for the commercial methanation in a fluidzed bed [29]. The most widely used catalyst for the commercial methanation of syngas is Ni based catalyst, modified with addition compounds such as MgO, Al_2O_3 and SiO_2. The modification of Ni catalyst with these oxides has shown to maintain the performance of the catalyst which would otherwise be deteriorated by the formation of carbon due to the dissociation of CO during the methanation [30]. It is reported that the life time of a catalyst could be between 3 and 10 years depending on the operating condition and the presence of impurities in the gas stream [31].

2.5 Gas conditioning

After the methanation process of the syngas, the gas stream contains mainly CO_2 (formed mainly due to water-gas-shift) and CH_4 (biomethane). The produced CO_2 can either be injected with H_2 to the Sabatier process for further enhancement of biomethane production or separated and ejected out to the atmosphere. With the choice of the former alternative, pure CO_2 (after separation) or with other gas can

be injected to the Sabatier process. The gas stream after the Sabatier reactor may contain unreacted CO_2 and H_2. These gases have to be removed from the gas stream in order to produce a standardized biomethane which will be ready to be injected to a gas grid to be utalized.

2.5.1 Sabatier process

The Sabatier reaction, first found by Paul Sabatier in 1910s, is an exothermic reaction where CO_2 reacts with H_2 to form CH_4 and H_2O, according to reaction 2.8. This reaction occurs in the presence of catalysts [32].

$$CO2 + 4\,H2 \longrightarrow CH4 + 2\,H2O \qquad \Delta H = -165\,\mathrm{kJ/mol} \tag{2.8}$$

The formation of carbon according to reaction 2.9, 2.10 and 2.11 also occurs during the Sabatier process. Carbon formation is dependent on the process temperature and pressure. At atmospheric pressure carbon forms at 365°C, and with increasing pressure its formation temperature also rises quickly. The formation of carbon during the process is undesirable because it gets deposited on catalyst and consumes the reactants, thereby decreasing the CH_4 yield. Therefore it is recommended the process is operated at higher pressure [33].

$$CH4 + H2 \longleftrightarrow C\,(s) + 3\,H2 \qquad \Delta\,H^{\circ} = 74{,}9\,\mathrm{kJ/mol} \tag{2.9}$$

$$2\,CO \longleftrightarrow C\,(s) + CO2 \qquad \Delta\,H^{\circ} = -172{,}4\,\mathrm{kJ/mol} \tag{2.10}$$

$$CO2 + 2\,H2 \longleftrightarrow C\,(s) + 2\,H2O \qquad \Delta\,H^{\circ} = -90\,\mathrm{kJ/mol} \tag{2.11}$$

The Sabatier process is thermodynamically bounded, and lower operating temperature in the range of 250-400°C is required for higher conversion of CO_2. Various studies have been done to investigate and compare the performance and selectivity of different catalysts, such as Rh, Ru and Ni, for the reaction [32]. Ni and Rh have been proven to be the most suitable and economically competitive catalyst used in the Sabatier process at industrial level [33].

2.5.2 Sabatier reactor

The two types of reactors used for the implementation of the Sabatier process are packed-bed (the traditional one) and the microchannel reactor. The microchannel reactor has an improved performance for the conversion of CO_2 as a result of the better mass and heat transfer between reactants and channel walls [34].

One major problem in the Sabatier process is the rise of temperature because of the exothermicity of the reaction. The increase in temperature in the reactor unfavour the formation of the product (CH_4 and H_2O) due to the deactivation of the catalysts at the temperature over 450°C [34]. Therefore the Sabatier reactor has to be designed so that the temperature in the reactor is controlled. Solar Fuel devised the Sabatier reactor in which at least two reactors are connected in series. In such reactor configuration the temperature of the reactor is controlled by inter-cooling

and condensation of the water which will be removed partially before the gas stream is reheated and enters into the next reactor. The partial removal of water favours the formation of CH_4. Turbo SE and MAN Diesel invented in 2011 an advanced single reactor for the Sabatier process. The reactor has two separate regions with shell-and-tube reactor which is filled by catalyst pellets. Each region of the reactor is cooled solely by cooling medium that flow externally on tubes [24].

The Sabatier process can be described by kinetic models such as power laws and Langmuir-Hinshelwood-Hougen-Watson LHHW. The process could be described by presenting a model for WGS and methanation of CO separately, or by a single model for the reaction 2.8 [24][33]. Schlereth [24] attempted to derive a kinetic model that reflects the Sabatier process (for reaction 2.8) at commercially acceptable conditions. He experimentally investigated the LHHW model for the Sabatier process when Ni-alumina is used as the catalyst of the process. Schlereth assumed the formation of formly functional group (HCO-X), as rate influencing factor, in the derivation of LHHW model. The descriptions of LHHW model, which can be formulated according to equation 2.12, is presented in Appendix A in detail.

$$r = Kinetic factor. \frac{Driving force}{Adsorption} \tag{2.12}$$

2.5.3 Carbon dioxide removal

There are different technologies to be used concerning the removal of CO_2 from a gas stream. These technologies are adsorption (pressure and temperature swings), absorption (using chemical solvents), membrane separation, cryogenic separation and biological fixation [35][36][37]. Of all these technologies chemical solvent absorption is the most reliable, widely studied and economically feasible method in the application of removing CO_2 from a gas stream . The most acceptable and widely used chemical solvent in the CO_2 scrubbing is the aqueous solution of monoethanolamine MEA[37][36][38]. In the MEA scrubbing process two fundamental reactions take place between amine and CO_2[38].

$$2\,R{-}NH_2 + CO_2 \longleftrightarrow R{-}NH_3{}^+ + R{-}NH{-}COO^- \tag{2.13}$$

$$R{-}NH_2 + CO_2 + H_2O \longleftrightarrow R{-}NH_3{}^+ + HCO_3{}^- \tag{2.14}$$

According to reaction 2.13 and 2.14, 2 moles and 1 mole of MEA, respectively, are stochiometrically required to absorb 1 mole of CO_2. Which means that the stochiometric absorption capacity of MEA according to reaction 2.13 and 2.14 is 0,36 and 0,72 $kgCO_2/kgMEA$. Studies have shown that the absorption capacity of MEA is dependent on operation temperature, presence of additional gases in the gas stream and the concentration of MEA in the aqueous solution. The presence of gases such as O_2, H_2S, HF, HCl, SO_2 and NO_2 in the gas stream degrade the absorbing capacity of MEA because these gases react with MEA to create unwanted

byproducts and reduce the absorption process' reaction rate [35][36][38]. Figure 2.5 illustrates the absorption process of CO_2 with chemical solvent [39].

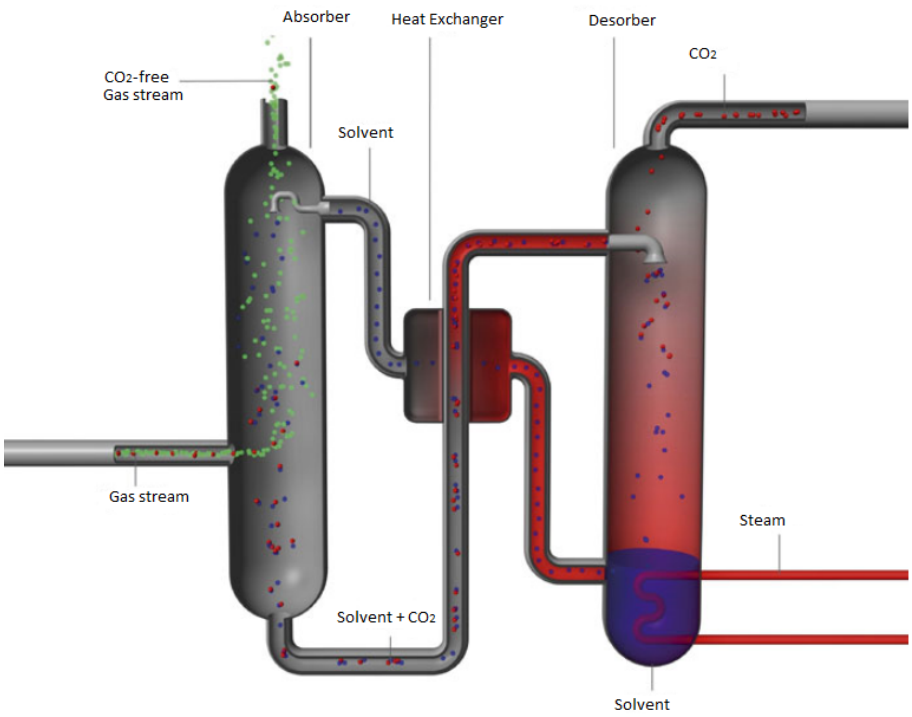

Figure 2.5: The absorption process of CO_2 with chemical solvent, adapted from [39].

As it is seen on Figure 2.5, the gas stream to be purified is fed into the absorber. The chemical solvent, at relatively low temperature, is streamed from above in the absorber so that it absorbs CO_2 from the counter flowing gas stream. The chemical solvent, rich in CO_2, is then transported to the desorber through the heat exchanger where it absorbs heat from the regenerated solvent. In the desorber, which constitutes the main energy demand of the absorption unit (over 70%), CO_2 is released from the solvent through stripping.

In order to design an optimal CO_2 scrubber experimental data for CO_2 absorption process is required [38]. Yeh et al.[36] did an experiment to investigate how the absorption capacity of MEA and the efficiency of CO_2 capturing are influenced by MEA concentration (7-35% w/w), CO_2 level in the gas stream (8-16% v/v) and operation temperature (10-40°C). It was shown that the MEA absorption capacity and efficiency varied between 0,36-0,38 $kgCO_2/kgMEA$ and 0,42-0,92, respectively, with the variation of MEA concentration while operation temperature and gas concentration were kept constant at 25°C and 16%(v/v) respectively. It was observed that the CO_2 absorption capacity and efficiency were slightly improved, 0,35-0,40 $kgCO_2/kgMEA$ and 0,88-0,94 respectively, with the variation of operation temper-

ature [36]. In an experiement done by Jose et al. [38] the absorption capacity of MEA is independent of the CO_2 concentration in the inlet gas stream, provided that the inlet gas stream is free from the toxic gases (O_2, H_2S etc) which would have otherwise jeopardised the proper functionality of the MEA.

Of the CO_2 removal technologies used in the framework of producing SNG, amine-based absorption is superior in giving high CO_2 removal and high CH_4 recovery (99,96%) [40]. It is reported that the thermal energy requirement when using 30% (w/w) MEA for scrubbing of CO_2 lies in the range of 3,2 - 5,2 MJ/kgCO_2 [35]. Heyne et al. [41] calculated the energy demand for the regeneration of MEA when removing CO_2 from biogas (30-55 vol-% in concentration of CO_2) to be 3,3MJ/kgCO_2 [41]. This energy is often provided by steam with a temperature in the range of 120-150°C. The loss of MEA during absorption process lies in the range of 0,3-0,8 kgMEA/ tonCO_2 [42].

2.5.4 Hydrogen separation

After the Sabatier process, there could be unreacted H_2 in the gas stream. In order to produce the biogas with the right Wobbe Index, the unreacted H_2 has to be removed. Pressure swing adsorption PSA is the most widely studied and used technology for H_2 purification at industrial level [43]. The principle of PSA is based on adsorption which arises when the gas molecules interacting with the neighboring solid (adsorbent) surface are physically bonded to the surface. The forces of attraction between the adsorbent material and the gas molecules is a function of the nature of the adsorbing material, operating temperature and the partial pressure of the gas component. In the case of the physical adsorption the determinant force is the van der Waals forces between the adsorbent surface and the gas molecules. Volatile gases such as H_2 and He are selectively not adsorbed in comparison with gases such as N_2 and CO_2 [43].

There are two pressure levels in the PSA system. The first is the high pressure level (usually between 10 and 40 bar) where the adsorption of undesired gases occur. The adsorption process continues until the equilibrium loading between the surface of adsorbent and contaminants are attained. When the adsorption process is completed, the desorption of impurities from the adsorbent material starts at lower pressure (slightly above atmospheric pressure), thus regenerating the adsorbent material. In such manner the PSA process cyclically swings between two pressure levels [44].

With PSA technology, 60-90% of hydrogen recovery can be achieved from a gas stream whose major constituent is hydrogen (around 50 vol-%) in the inlet stream. In this manner hydrogen purity of 99,99% can be achieved. If the level of the impurities in the gas stream is low, temperature swing adsorption (TSA) is the advantageous way to purify hydrogen. In the TSA process, the system works between two different temperatures [44].

The most widely used adsorbents in hydrogen purification, depending on the operation temperature and pressure, is silica gels, aluminas, zeolites and activated carbons. The usage of these adsorbents is also a function of the type of impurities needed to be removed. Activated carbon, for example, is a very effective adsorbent in removing H_2 from a mixture of CO_2 and hydrocarbons, but they are less advantageous when it comes to separating H_2 from a gas stream of CO and N_2 [45].

From the data published by Mivechian et el. [46] in the study of hydrogen separation from off-gas streams (72 and 25 vol-% of hydrogen and methane respectively) using PSA technology at the Tehran refinery plant, the electric energy demand of the PSA system was calculated to be 0,53kWh/kgH_2 [46].

2.6 Power-to-gas technology

In the concept of power-to-gas (P2G) technology, electric energy, through different applications, is converted into gas that could be stored and used as fuel. The most common application of P2G technology in the gasification process is to produce H_2 and O_2 through electrolysis according to reaction 2.15. The produced H_2 can be made to react with CO_2 of the product gas according to the Sabatier reaction to produce biomethane [47].

$$2\,H_2O \longrightarrow 2\,H_2 + O_2 \qquad \Delta\,H^{\circ} = 286\,\mathrm{kJ/mol} \tag{2.15}$$

The other application of P2G technology is the direct heating of a gasifier by resistance heater which converts electric energy into heat energy. This would decrease the internal energy demand of the gasifier and leads to the decrease of char combustion and increases char gasification instead. The advantage of this application over the electrolysis is that it has a higher efficiency , because more amount of energy is stored in the product gas, and lower investment cost [7].

The electricity used in the P2G technology could come from the intermittent renewable energy sources such as solar and wind energy whose installed capacity is continuing to increase. The integration of these renewable energy risks the stabilization of electric grid due to its alternating nature. Therefore a widespread research is being done as to how to fully utilize the potential of these energy sources while maintaining the stability of the grid. P2G technology is a suitable candidate that has got attention in this regard. In water electrolysis, electrical energy is used to turn water into its elemental components H_2 and O_2, which can be stored/used to produce biomethane that can be injected to the existing gas grid. This, furthermore, increases the attractiveness of P2G technology application as it makes use of the already existing gas network [48]. Additionally, these intermittent energy sources are suitable candidates to work in synergy with direct gasification because the oxygen produced through electrolysis can be used as a gasifying agent.

2.6.1 Electrolyser

The core of P2G technology is the electrolyser which through electrolysis converts electrical energy and water into H_2 and O_2. There are three types of electrolysers: alkaline, PEM (polymer electrolyte membrane) ans SOEC (solid oxide electrolyser). The first two electrolyser technologies are currently being used both at pilot and commercial level for water electrolysis. They are called lower temperature electrolysers because they operate below 100°C. On the other hand, SOEC operates at higher temperature and has energy efficiency of 90-95%. However, SOEC technology is not accessible for the commercial application yet as it is still at the research stage [47]. The efficiency of an electrolysis technology can be described according to equation 2.16

$$\eta_{efficiency} = \frac{LHV_{H_2}}{E_{electricity}} \tag{2.16}$$

where $\eta_{efficiency}$ is the electrolytic efficiency, LHV_{H_2} is the lower heating value of hydrogen and and $E_{electricity}$ is the amount of energy used in the electrolysis.

Among electrolysis technologies, alkaline is considered to be the most mature and cheap technology which is used at the industrial level. Aqueous potassium hydroxide, steel and nickel-plated steel are respectively used as electrolyte, cathode and anode in the akaline electrolyser. The main drawbacks related with the usage of alkaline electrolyser is that it has limited operational pressure (below 30 bar), limited range of load and environmental problem as a result of the used caustic electrolyte. With having the limited range of load, alkaline electrolyser has been considered to be unfit for the application in the P2G technology due to the varying nature of power output from intermittent renewable resources. However, alkaline manufacturers recently claimed to have designed the electrolyser that can adapt itself with ranging load of 5-100% of nominal capacity with increased hydrogen production and fast starting time in the range of seconds [47].

PEM electrolyser is an electrolysis technology used at both commercial and pilot level. This technology is developed to overcome high pressure operation (up to 100 bar) and partial load (as low as 5%) which alkaline electrolyser suffers from. In PEM electrolysis, a polymer membrane which is proton conductive material is used as an electrolyte. The polymer lso helps to separate the product gases. Conventionally, platinum alloy (with either ruthenium or iridium) and platinum is used as anode and cathode respectively. The usage of this material increases the investment cost and durability of the PEM electrolyser in comparison with the alkaline. Table 2.3 shows the specification and operation parameters of alkaline and PEM electrolysers [47].

Table 2.3: Alkaline and PEM electrolysers' specification. The economy of the electrolysers applies for 2016 [49][50][51][52].

Specification	Alkaline	PEM
Capacity range (Nm^3/hr)	301 – 485	100 - 400+
Production capacity (% of nominal flow rate)	20 – 100%	0 – 100%
H_2 yield (kg/MWh_{el})	23,7	18,69
H_2 purity	99.9% ± 0.1	99.99%
Efficiency (LHV)	40-70%	48-72%
Investment cost (€/MW)	1,07	2,55
Operating cost (% of inv.cost)	4	4
Life span (year)	25	20

2.7 Intermittent electricity in Sweden

The annual production of electricity in Sweden is normally between 140 and 150 TWh, with hydroelectric power and nuclear power being the dominant electricity producers in the country [53]. However, driven by the energy policy (in the form of subventions, researching and electricity certificate system) the share of renewable energy resources in the total electricity supply of the country is increasing. Wind and solar power, which are intermittent energy sources, are the main sources of electricity production that are increasing significantly.

Wind power is a renewable energy source and it exists over the whole country. In the year 2000, the installed wind power in Sweden was 241 MW, covering 0,2% of the total electricity of the country. However, the installed power raised to around 6000 MW in 2015, covering about 16 TWh, 10% of the total electricity supply [54]. The installed power is expected to rise as the governmen pushes toward the Swedish goal of 30 TWh (approximately 20% of the total electricity) energy from wind power by the year 2020. Figure 2.6 shows the exponential increase in the electricity supply from wind power between 2003 and 2015 [55].

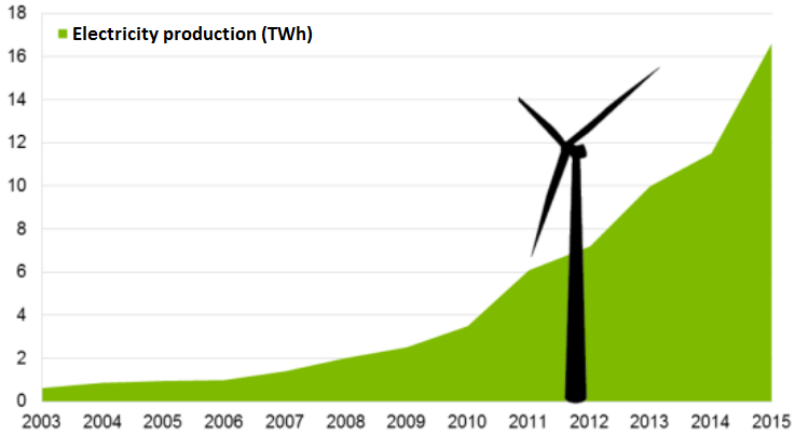

Figure 2.6: The increase in electricity supply from wind power between 2003 and 2015 [55].

Solar power on the other hand is a renewable energy source which has got considerable attention in the move to change the energy system of the country to be more renewable. Even though Sweden is located far from the equator, the region on Earth which receives highest solar energy, an installed solar power of 1 kW in Sweden give rises to an annual energy production of 1000 kWh, according to the right-hand rule [56]. This amount of solar power installation require an area of 7 m^2. As for 2016 there was around 200 MW of solar power installed in Sweden, producing 0,2% (0,3 TWh) of the total electricity supply, and the political ambition from the Swedish Energy Authority was to increase the energy production from solar power to 7 - 14 TWh [56].

In order to create awareness and thereby increase the private usage of solar power in residential houses and villas, the Swedish government has introduced in 2015 the tax reduction for the private installation of solar power. The reduction meant that the micro-producers receive the payment of 60 cent/kWh for the excess solar energy they feed into the electric grid. Figure 2.7 illustrates the cumulative installed solar power in Sweden between the year 1992 and 2015. The total installed power of each year is divided according to the type of the systems to which the power is connected to [57].

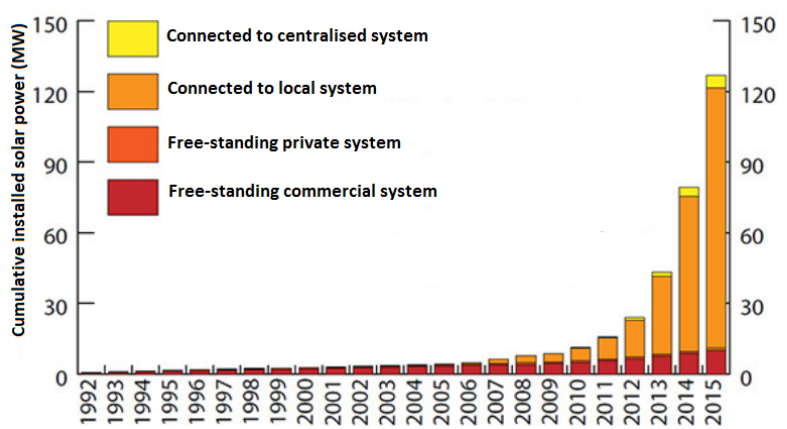

Figure 2.7: The installed cumulative solar power from 1992 to 2015 in Sweden [57].

The amount of electricity produced at every moment has to be equal with the amount of electricity consumed at that moment. Otherwise the frequency of the system cannot be kept at 50 Hz. The increase in the electricity production from wind and sun, in a sense, contributes to a sustainable development. However, the intermittent nature of these sources destabilise the frequency of the electric grid.

3
Methods

3.1 Modeling in ASPEN PLUS

ASPEN PLUS is a computer program that can be used to simulate a gasification process. It helps to model and simulate biological, physical and chemical processes that concern gaseous, liquid and solid streams under defined settings [12]. Using computer program for simulation and modeling of a process is more cost effective than carrying out experiments, even though not always as accurate. Furthermore, computer simulations can also help to answer different questions that cannot be answered by experiments.

3.1.1 Gasification modeling

Modeling of a gasification process in fluidized bed is primarily implemented with two modeling ways: dynamic and equilibrium modeling. The dynamic modeling of a process is done by taking the kinetics of reactions and hydrodynamics (reactor's geometry and design with the residence time of the gas) of the reactor into consideration. Fulfilling the detail of all parameters required by the dynamic model could be complex and tedious, but the model gives an acceptable reflection of a real process. In the equilibrium modeling, only thermodynamic concepts of the process is treated, and modeling with such approach is advantageous for exploratory design and process development [2][58].

The simulation and modeling of biomass gasification, using ASPEN PLLUS, in a fluidized bed have been done by [9],[12],[13],[28],[58] and [59] among others. In these studies, a far-reaching kinetic models of gasification were developed and certified with the experimental data. When modeling the gasification system, it is common that different steps of gasification, drying, pyrolysis, volatile combustion and char gasification are separately modeled. It is common that part of the gasification process such as pyrolysis and combustion of volatiles are modelled with equilibrium model, assuming the produced species can attain the minimum Gibbs free energy. Different types of approaches are taken when it comes to tar modeling. The common assumptions made for tar modelling is that it is considered either to be inert or represented by heavy cyclic hydrocarbons such as benzene, toluene and naphthalene [12]. For the simulation of gasification process in the ASPEN PLUS program, different types of components are used. Table 3.1 presents types and model of components with descriptions as to why/when they used [60].

Table 3.1: Some of the components, with their model and descriptions, that can be used in ASPEN PLUS for a gasification system [60].

Model	Description	Purpose
		Reactors
RStoic	Stochiometric reactor	Helps to model stochiometric a reactor with known reactions, kinetics is not important here.
RYield	Yield reactor	Helps model a reactor with known yield distribution, stochiometry and kinetics are not important.
REquil	Equilibrium reactor	Helps to model a reactor with simultaneous chemical and phase equilibrium.
RGibbs	Equilibrium reactor with minimization of Gibbs free energy	Helps to model a reactor with phase and chemical equilibrium with minimized free Gibbs energy. It Calculates phase equilibrium for vapor-liquid-solid systems and solid solutions.
RCSTR	Continuously stirred reactor	Helps to model a reactor which is continuously stirred in one-, two- or three-phase, with known kinetics and stochiometry.
RPlug	Plug flow reactor	Helps to model a reactor which is one-, two- or three-phase plug flow reactors, with known kinetics and stochiometry.
		Separators
Sep	Component separator	Helps to separates inlet stream into different outlet streams according to specified fraction or flows.
Flash2	Two-outlet flash	Helps to separates inlet stream into two output streams by using rigorous vapor-liquid-liquid or vapor-liquid equilibrium.
		Heat Exchangers
Heater	Heater or cooler	It is used as a heater, a cooler or a condenser. It determines phase and thermal conditions of output stream.
HeatX	Two-stream heat exchanger	It helps to exchange heat between two streams.

3.2 Model development

The process simulation is carried out by flowsheeting in ASPEN PLUS, beginning with the handling of wet biomass to the production of the end product, biomethane. The whole process is divided into different stages: drying, gasification of biomass, syngas cleaning, methanation of the product gas and the Sabatier process where the CO_2 of the gas stream after the methanation reactor is made to react with H_2 for four different scenarios. Thus, only the Sabatier reactor configuration differ between all the models.

In the simulation, the $PR - BM$ (Peng-Robinson equation of state with Boston-Mathias modification) property method was used to calculate the physical property of conventional components, while the DCOALIGT and HCOALGEN (property model for the non-conventional components) are used to calculate the density and enthalpy of non-conventional components (biomass, ash and char). The ultimate and proximal analysis of the biomass (forest residues) used in the model are given in Table A.5 and Table A.4 in Appendix A respectively.

3.2.1 Biomass drying

Assumptions: Pressure drop in the dryer is neglected. The drying process is isothermal and in steady state.

Figure 3.1 is the representation of the ASPEN PLUS model of the belt dryer as proposed by Alamia et al. [10]. The RStoic reactor, AIRDRYER, represents the air belt of Figure 2.3 where the hot air is blown over the biomass, drying the biomass to a certain level. The partially dried biomass is transported further to be dried by the two consecutive RStoic reactors, DRYER1 and DRYER2, which represent the steam belt dryer. More in detail, in the RStoic blocks, the biomass moisture properties are changed while water is generated accordingly and separated afterwards in the separator blocks. The drying agent (steam) is represented in the subsequent steam cycle where the energy duty is also calculated and where the biomass moisture is first injected and then purged out. The stream DRYB contains biomass with the moisture content of 10.4% which will be transported to the gasifier.

Alamia et al. [10] calculated using CFD the required energy to dry 1 kg of biomass, from a given moisture content to the desired moisture content, in the belt dryer they proposed. Based on the presented calculation, the amount of energy required as a form of hot air and steam to dry the biomass from 40% to 10,4% moisture content was determined.

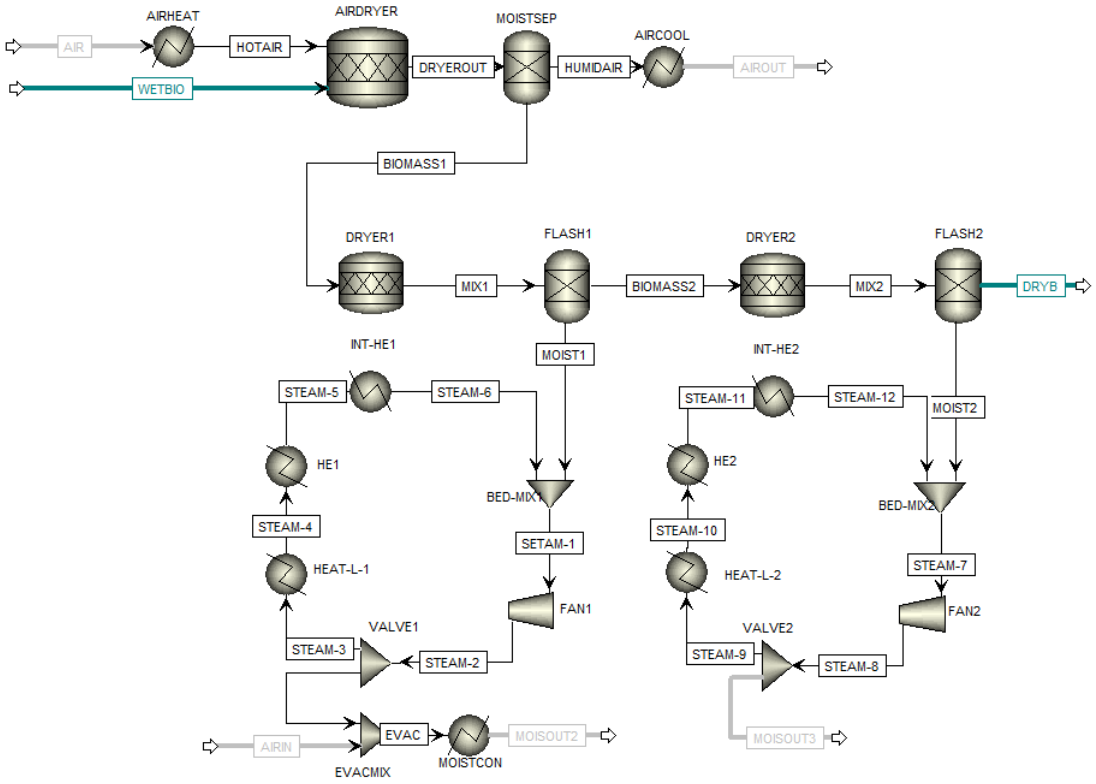

Figure 3.1: The ASPEN PLUS model of the belt dryer. The acronym of components and streams with their descriptions are given in Table B.1 in Appendix B.

3.2.2 Gasification process

Assumptions: Pressure drop in the gasifier is neglected. The gasification process is isothermal and attains steady state. Devolatalization takes place instantaneously. The formed tar is assumed to be disintegrated into CO and H_2 by an ideal catalyst. Costs for cleaning the syngas from particulate matter is negligible.

As illustrated in the theory section, gasification is a complex process, the modelling of which would require detailed reaction kinetics and well defined operational parameters such as internal local temperature and pressure, feedstock particles size and shape etc. Our modelling approach was aimed to reproduce the exact experimental data of an existing direct gasifier running on similar biomass and using identical operational conditions. We set an atom balance and we adjusted the inlet parameters accordingly, being confident that the experimental results would lay in a safe 10% error margin: we imposed the results of our model to be identical to the experimental data but, at the same time, we changed the inlet parameters of air-to-fuel and steam-to-fuel ratio in order to match the atom balance, assuming that, in a real case, the small adjustments in the inlet parameters would not have led to a deviation in the results greater than 10%. Figure 3.2 shows how the simulation was imposed to mimic the experimental results.

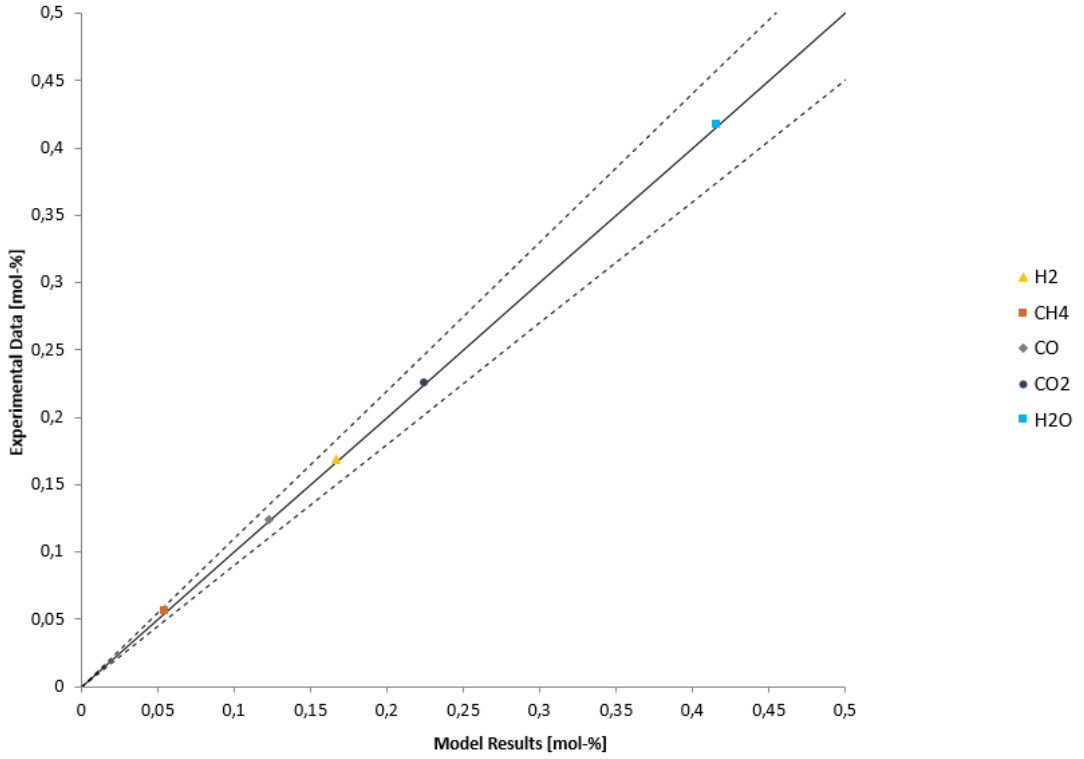

Figure 3.2: Comparison between experimental and the model-produced gas compositions for the main gas components of the product gas. The two dotted lines enclose the region of 90% confidence around the linear line of slope 1.

Figure 3.3 depicts the developed gasification process that reproduces the experimental data of the wet gas composition from gasification of forest residues as it is presented in Hannula et al. [9], see Table B.4 in Appendix.

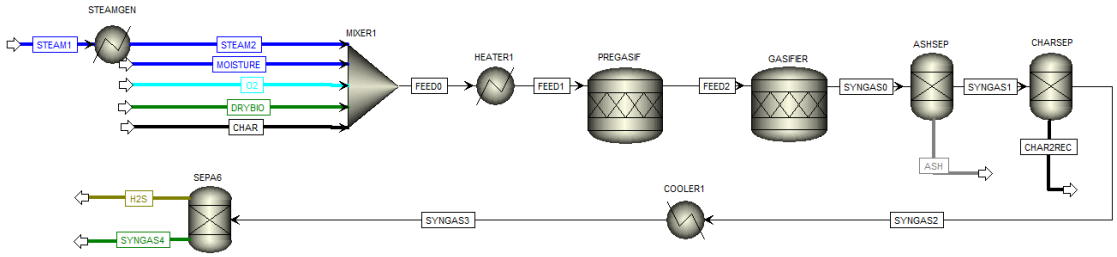

Figure 3.3: The ASPEN PLUS model of the biomass (forest residues) gasification. The process is operated at the pressure of 2,5 bar. The acronym of components and streams with its description are given in Table B.5 in Appendix B.

As it can be seen on Figure 3.3 two RStoic reactors with acronym PREGASIF and GASIFIER are used. PREGASIF is used to decompose the dry biomass into its elementary constituents according to reaction 3.1. The coefficient of the products are

calculated by dividing the molar amount of the component in the biomass with the amount of dry biomass feed. In GASIFIER, the product from PREGASIF together with other inputs (steam, oxygen, biomass moisture and char) reacts to produce the wet gas composition of the experiment as it is presented in Table B.4 (the modified column). The produced gas at the temperature of the gasifier is cooled down after ash and char have been removed by ideal separators. H_2S is then separated from the produced gas. In the modeling, 97% of carbon conversion is assumed, and the char (which contains C, H_2, and O_2 in the w-% of 97, 1 and 2 respectively) is recycled. Table B.3 in Appendix B shows the variables and their value used in the model of Figure 3.3.

It was possible to represent the gasification process with one RStoic reactor only; thus letting the whole process be represented by a single reaction where reactants are biomass, steam and oxygen, and the products are the wet gas composition from the experiment. However, the single reactor case simulation did not match the energy released during the decomposition of biomass with LHV of the dry biomass. The reason could be that ASPEN PLUS might not correctly determine the heat of reaction for the non-conventional component, biomass. Therefore, in order to solve this issue, the energy duty required in the reaction turning the biomass into its elemental components was calculated as follows:

1. the complete combustion of the biomass was modeled through 2 RStoic blocks, one to decompose the biomass into its elements and the other to combust these elements. The energy duty of the RStoic block in charge of the oxidation was reliable (since the reactor is operating with all ASPEN PLUS conventional materials), while the heat of the reaction for the biomass degradation into its elements was manually adjusted until the overall energy duty of the process corresponded to the actual LHV of the fed biomass.
2. the same heat of reaction calculated in the first RStoic was then used in the analogous RStoic (PREGASIF reactor) block in the gasification model.

$$\begin{aligned} \text{BIOMASS} \longrightarrow\ & 0{,}0427108\,\text{C} + 0{,}0123291\,\text{O}_2 + 1{,}5585\,\text{e-005}\,\text{S} \\ & + 0{,}000178396\,\text{N}_2 + 0{,}0302597\,\text{H}_2 + 0{,}025987\,\text{ASH} \end{aligned} \tag{3.1}$$

3.2.3 Syngas cleaning and pre-methanation

At the end of the gasification process the product gas is still not ready to be processed in the metanation section. Impurities (such as H_2S) and ash have to be removed. Char has to be removed and recycled, and the gas has to be compressed to the methanation reactor's operational pressure which in this model is between 14 and 10 bar. These steps occurs in series according to the following order:

1. ash removal;
2. char removal and recycle;
3. gas cooling (till the temperature required for the H_2S scrubbing);
4. H_2S scrubbing by using aqueous MDEA solution (15 wt%);
5. liquid phase separation (for a more efficient compression);
6. gas inter-refrigerated compression, liquid phase and condensate compression.

The liquid phase and the condensate are mostly water and their re-injection inti the methanation process can be dosed and optimized according to the reaction needs (for example in the water-shift reaction).

3.2.4 Methanation (Base case)

Assumptions: The process is isothermal and attains steady state with thermodynamic equilibrium while keeping the minimum Gibbs free energy. There is pressure drop in the process.

Figure 3.4 depicts the flowsheet where the cleaned syngas (product gas) from the gasifier is dried and pressurized for methanation. As it is seen on the figure, four RGibbs reactors are seriously connected as it has been described in the literature [23][28]. The configuration of reactors, also, resemble that of which Alamia et al. [61] used for the simulation of methanation process of the GoBiGas plant.

The first reactor of the methanation process is set so that the the water-gas-shift (WGS) takes place, consuming CO and boosting the H_2 content of the gas stream. This is done by implying restricted chemical equilibrium with specified temperature approach of 5°C while keeping certain species such as N_2, S, H_2S and C and all hydrocarbons inert. The remaining RGibbs reactors are set with calculated phase and chemical equilibrium while specifying possible products (all components in the inlet gas are assumed to be present in the product). In these reactors the methanation of CO (reaction 2.7) occurs. RGibbs reactors, by keeping the minimum Gibbs free energy, resembles the methanation process in the fluidized bed which gives higher heat transfer and turbulence that favors the reactions. Since the reactions occurring in this process are exothermic, inter-stage cooling has been performed to restore the process temperature as the driving force of the reaction. The outlet gas temperature after each reactor was monitored so that it lies in the recommended range of 250-700°C.

In the methanation process of Figure 3.4 the pressure drops from 14 bar at the inlet of HEATER2 to 10 bar at the outlet of COOLER6. The pressure drop only occur in the heat exchangers. Heat duty for all the reactors are set to be zero, and activation energy for the reactants at the inlet of of the first reactor was provided by a heater. Table B.7 in Appendix B presents the variables and values used in the simulation of methanation process as it is depicted in Figure 3.4.

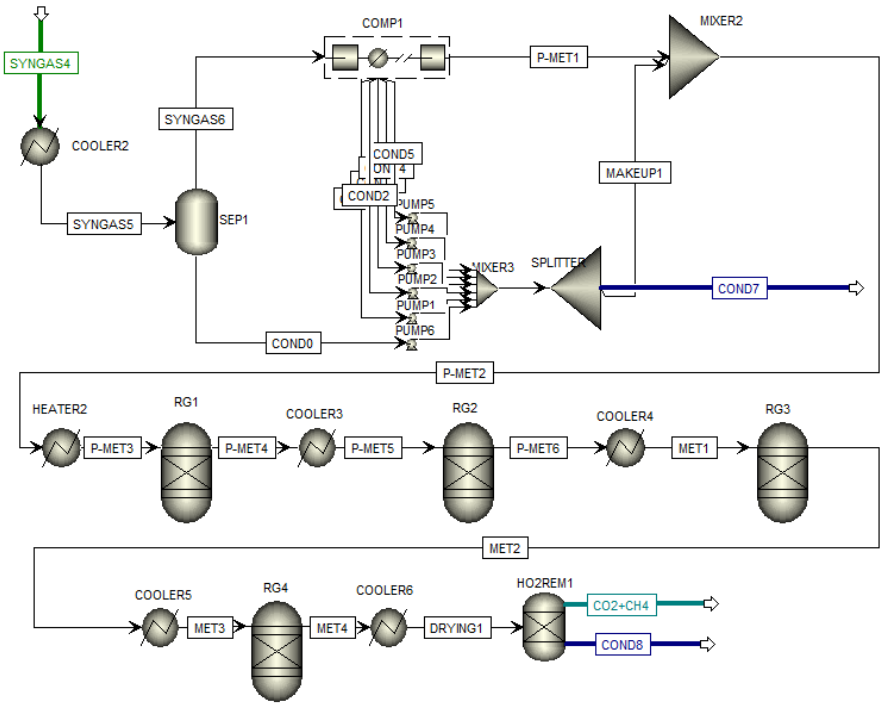

Figure 3.4: The BaseCase ASPEN PLUS model for the methanation of the product gas. The acronym of components and streams with its description are given in Table B.6 in Appendix B.

3.2.5 Sabatier process

In the methanation reactor, both the WGS (reation 2.6) and the Sabatier reaction (reaction 2.8) occur. However, the high operation temperature of the methanation reactor (250-700°C [23]) favor the rate of WGS much more than the Sabatier reaction, thus resulting in the accumulation of CO_2 in the gas stream at the end of the reactor. The gas stream after the methanation reactor predominantly contains H_2O, CO_2 and CH_4.

In order to produce the standard biomethane according to Table 1.1, the gas product of the methanation reactor has to be dried. The CO_2 has to be removed or the dried gas stream has to be further sent to a separate Sabatier reactor so that the CO_2 will react with the supplied H_2, enhancing the production of biomethane. In this case, the later option has been chosen, and the hydrogen sources for the Sabatier reactor are assumed to be two electrolyzer technologies: alkaline and PEM.

Microchannel reactors give better yield for the Sabatier process [32]. Therefore the simulation of the process here is represented by multi-tubular Rplug reactor, which also has been used by Jürgensen et al. [33] for the simulation of the Sabatier process, with specified temperature according to Figure 3.5, see Table C.4 in Appendix C for the setting of the reactor.

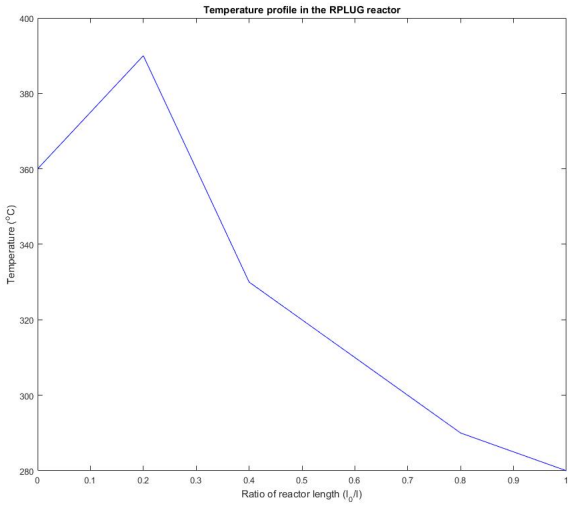

Figure 3.5: The temperature profile in the RPLUG reactor of the Sabatier process.

The temperature range, on Figure 3.5, favors the carbon conversion of the Sabatier process [32], and the risk of carbon formation in the reactor with this operation temperature is negligible because the reactor is operating at the elevated pressure of 60 bar [33].

The Sabatier process is modeled kinetically based on LHHW model according to equation 2.12. The values for adsorption constants, equilibrium constants and kinetic factor given in Table A.1 and A.2 in Appendix A are used to model the process. The reactor size is automatically updated with the flow through an internal code. Moreover, in order to achieve the same rate of reaction for different inlet flow conditions, the reactor has been always oversized; nevertheless the volume variation with the flow has been considered so that it is possible to asses the magnitude of the investment cost variation accordingly.

Four different layouts, called scenarios, are developed for the simulation of the Sabatier process. Upstream, all the scenarios have the same gasifier and methanation reactor (base case). The operational parameters (such as pressure, temperature, catalyst type load and density) are the same for every scenario. In all the scenarios, heat exchangers HEATER3 and COOLER7 are placed respectively before and after the Sabatier reactor. The former ensures that the temperature of the stream entering the RPlug reactor is high enough to trigger the reaction in a reasonable time while the latter cools down the product stream so that the condensate can be then easily removed by the separator H2OREM2. A turbine is placed immediately after the RPLUG reactor to lower the pressure of the outlet gas stream to 10 bar so that the CO_2 removal columns that may come in the downstream process will perform at a plausible pressure. In all the scenarios, the produced biomethane is pressurized to 30 bar by COMP3 in order to fulfill the gas grid standards and be subsequently injected into it.

The difference between the scenarios lies in the way the injection and ejection of CO_2 and H_2 are handled. The variables used, with their respective values, in the simulation of all the scenarios are presented in Table C.4 in Appendix C.
The produced biogas compositions must fulfill the standards of the Wobbe Index in order to be sold and other specifications, see Table B.8 in Appendix B.

3.2.5.1 Scenario 1

In this scenario, a mixture of dried gas (contains mainly CO_2 and CH_4) from the methanation reactor and H_2 from electrolysis are pressurized and then sent to the Sabatier reactor. The unconverted CO_2 is removed using two separators (each at 90% efficiency of CO_2 recovery), and some amount of CO_2 can be recycled to the inlet gas stream increasing the plant operational flexibility, while the rest is ejected to the atmosphere. Biomethane is produced to be pressurized to 30 bar by COMP3 and injected into the gas grid.

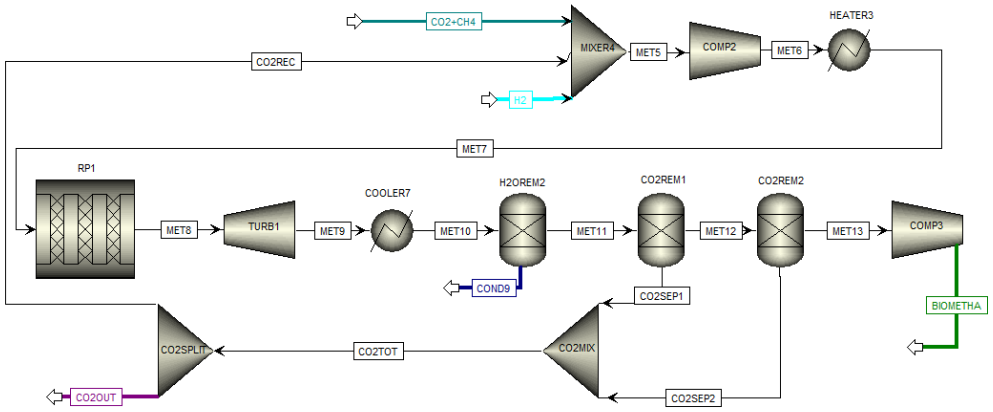

Figure 3.6: The ASPEN PLUS model for the simulation of the Sabatier process, Scenario 1. The acronyms of components and streams with the respective descriptions are given in Table C.1 in Appendix C.

3.2.5.2 Scenario 2

The dried gas stream of CO_2 and CH_4 from the methanation reactor together with the stream of H_2 is mixed and pressurized to be sent to the reactor. In this scenario, the H_2 feed is so that all the CO_2 in the inlet gas stream is completely converted. In this way, the CO_2 separator is no longer required and the CO_2 emission are minimized, however, this will necessitate the removal of the unreacted H_2 later in the downstream, since an excess amount of H_2 is required to enhance the driving force of the reaction equilibrium towards the products for the complete conversion of CO_2.

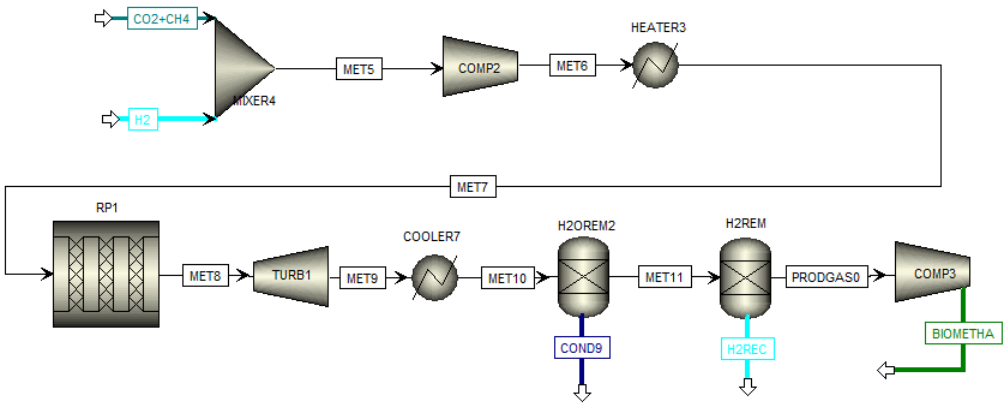

Figure 3.7: The ASPEN PLUS model for the simulation of Sabatier process, Scenario 2. The acronyms of components and streams with the respective descriptions are given in Table C.1 in Appendix C.

3.2.5.3 Scenario 3

In this scenario, 99% of CO_2 is recovered from the inlet gas stream, then only the decided amount is sent to the Sabatier process, providing operational flexibility to the layout and allowing a better size optimization of the reactor. The CO_2 is removed both from the products of the methanation and the Sabatier processes in the same unit after that the two streams have been mixed. Removed the CO_2, the gas is compressed according to the grid standards and then is ready to be sold. Furthermore, this layout consists also of a H_2 separator located downstream the Sabatier reactor, in order to achieve the maximum operational flexibility.

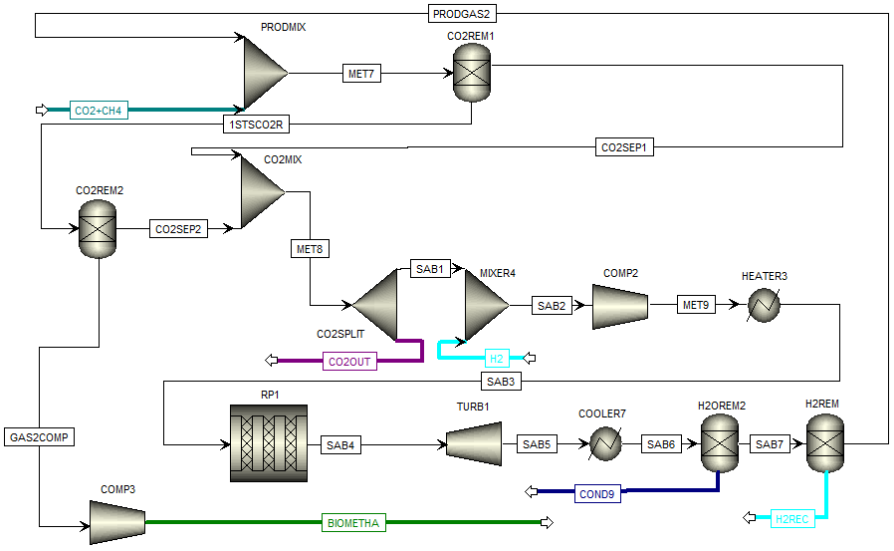

Figure 3.8: The simulation of the Sabatier process in ASPEN PLUS according to scenario 3. The explanation to acronyms of components and streams are given in Table C.3 Appendix C.

3.2.5.4 Scenario 4

In this scenario, the dried product stream of the Sabatier process is recycled and mixed with the gas stream from the methanation reactor whereafter CO_2 is recovered and injected to the Sabatier process. Scenarios 3 and 4 are identical, but Scenario 4 has no H_2 removal. It was interesting to find out how the increased flexibility in terms of being able to remove H_2 will affect the economic performance between the scenarios.

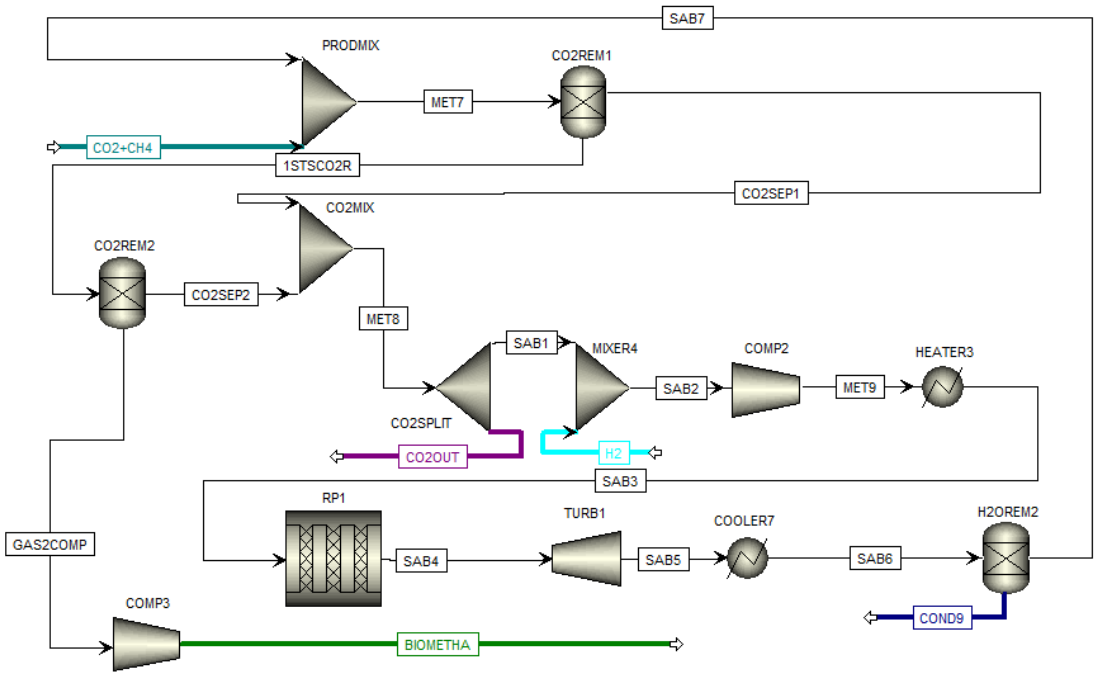

Figure 3.9: The ASPENPLUS model for the simulation of scenario 4. Descriptions to the acronym of streams and components are given in Table C.3 in Appendix C

Table 3.2 summarize the main features of different scenarios and their operational flexibility.

Table 3.2: Feauters of different scenarios.

Scenario	**Sabatier reactor's inlet stream**	CO_2 removal	H_2 removal	Flexibility	NO CO_2 emission after the methnation
1	CO_2 and H_2 and other gases	YES	NO	LOW	POSSIBLE
2	CO_2 and H_2 and other gases	NO	YES	NONE	YES
3	Only CO_2 and H_2	YES	YES	VERY HIGH	POSSIBLE
4	Only CO_2 and H_2	YES	NO	HIGH	POSSIBLE

3.3 Performance indicators

All the scenarios, except for scenario 2 where CO_2 was meant to be fully converted, were simulated while the amount of CO_2 and H_2 injection to the Sabatier process are independently varied. The H_2 injection was varied in the range of 0-24 kg/hr, which is actually a range that exceeds the value needed to the complete conversion of CO_2 for the given dry biomass feed of 100 kg/hr.

3.3.1 Thermodynamic performances

For the methanation reactor (BaseCase), a thermodynamic performance called methane efficiency η_{CH4} is defined according to equation 3.2. The methane efficiency indicates the energy in the dry biomass that can be recovered as a form of biogas after gasification.

$$\eta_{CH4} = \frac{(\dot{m} * LHV)_{CH_4}}{(\dot{m} * LHV)_{biomass}} \tag{3.2}$$

where ṁ and LHV are mass flow and lower heating value respectively, with the indices CH_4 and biomass standing for methane and biomass.

In order to compare the thermodynamic performance of the four scenarios, three different types of efficiency namely cold gas efficiency η_{cold}, overall system efficiency η_{system} and exergy efficiency η_{exergy} whose mathematical descriptions are presented in equation 3.3, 3.4 and 3.5 respectively, were defined.

$$\eta_{cold} = \frac{\sum(\dot{m}_p * LHV_p)}{\sum(\dot{m}_f * LHV_f)} \tag{3.3}$$

where ṁ stands for the mass flow of a component and p respective f being the product (CH_4 and H_2) and the feed (dry biomass and the injected H_2).

$$\eta_{system} = \frac{\sum(\dot{m}_p * LHV_p) + \dot{Q}^- + \dot{E}^-}{\dot{m}_{biomass} * LHV_{biomass} + \dot{Q}^+ + \dot{E}^+} \tag{3.4}$$

where $\dot{Q}$ and $\dot{E}$ are the thermal power (at 400K) and the electrical power, respectively. The plus (+) and minus (-) signs stand for the consumption and production respectively. The electrical power considered in the calculation was that of fans, compressors, PSA, electrolyzer and the turbine, while the thermal energy consumed was used for CO_2 and H_2S scrubbing.

$$\eta_{exergy} = \frac{\sum_p \dot{n}_p * e_p + \dot{Q}^-_{exe} + \dot{E}^-}{\sum_f \dot{n}_f * e_f + \dot{Q}^+_{exe} + \dot{E}^+} [62] \tag{3.5}$$

where ṅ and ė is the molar flow (kmol/s) and the corresponding standard exergy content (MJ/kmol), while index f and p stand for the net feeds and net products respectively. $\dot{Q}_{exe}$ is the exergy of the thermal power at 400K which can be calculated by multiplying $\dot{Q}$ with τ (defined by equation 3.6). The standard exergy of the component in the feed and product are given in Table A.3 in Appendix A, and the

molar flow of the of different components considered in the calculation are retrieved from simulations.

$$\tau = 1 - \frac{T_a}{T_i} \tag{3.6}$$

where T_a is the annual average temperature in Göteborg 281,15K [63] and T_i is the temperature at which the heat is transferred (in the case of the steam produced, for example, T_i is 400K).

Throughout the gasification model developed, from the feeding of the wet biomass into the dryer to the production of biomethane at the end of the Sabatier process, there are hot and cold streams. Therefore, to know the net heat flow in the process, it was necessary to draw a Grand Composite Curves GCC which shows the net heat flow against the temperature (shifted).

3.3.2 Economic performance

For the comparison of different scenarios from economic point of view, operational profits are considered. The operational profits are the subtraction of costs (money spent to buy biomass, electrical energy to operate the plant and to upgrade the biomethane in the methanation and Sabatier reactors) from the revenues (money received from selling biomethane, excess heat, by product oxygen and electricity). Operational parameters such as ash and char handling, bed-material regeneration, energy for biomass, oxygen and steam feeding, and tar scrubbing are not included here. Hydrogen is assumed to be supplied at the necessary pressure. Operational profits (as revenues-costs) are calculated using equations D.1-D.16 in Appendix D.

4

Results and Discussions

In this chapter the simulation results of the BaseCase and all the scenarios are presented with illustrating graphs. The cases are compared and contrasted according to performance indicators: thermodynamic performances with different types of efficiency (system, cold and exergy), and economic performance (operational profits and biogas production), while varying the injection of H_2 and CO_2 into the Sabatier process. The presented graphs shows the performance of the scenarios while producing the biogas according to the Wobbe Index of Table B.8 in Appendix B, thus only economically valuable biogas is considered.

4.1 Performance of the methanation (base case)

Using data from the simulation, the methane efficiency η_{CH4} and system efficiency η_{system} calculated according to equation 3.2 and 3.4, respectively, are 0,65 and 0,80. This values are not affected by the choice of the downstream plant layout (the Sabatier unit). Moreover, we use these values to compare direct and indirect gasification: since no hydrogen from water electrolysis is utilized so far these performance indicators are mainly affected by the gasification technology utilized (the indirect gasification plant we used for the comparison was not integrated with a unit for water electrolysis). The methane efficiency in this case, is higher than that of the indirect gasifier simulated by Alamia [7], which is 0,57. The higher methane efficiency of the direct gasifier is due to the production of good syngas composition which can be attributed to the use of oxygen as gasifying agent. However, the system energy efficiency calculated, 0,80, is lower than that of Alamia's which is around 0,9. It is clear that oxygen production penalized the over all system energy of the direct gasifier. Nevertheless, in this project, no use has been found for the excess heat available at a temperature lower than 400K, otherwise, the system energy efficiency will increase if the heat at lower temperature is considered valuable.

Given the exothermic nature of this process no external heat is required. Figure 4.1 shows the unpinched grand composite curve (GCC) of the BaseCase.

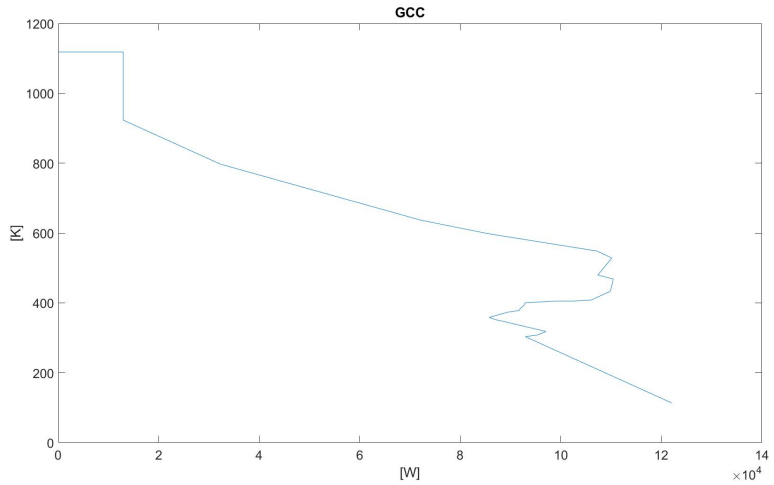

Figure 4.1: The unpinched grand composite curve of the BaseCase.

4.2 Thermodynamic performance of scenarios

4.2.1 Efficiencies with alkaline Electrolyzer

Since scenario 2 has no flexibility with respect to the hydrogen feed, it was compared separately. Figure 4.2 depicts the system energy efficiency for Scenario 1, 3 and 4, when H_2 is supplied by an alkaline electrolyzer. The intervals reflect the gas production fulfilling the standards required by the Wobbe Index. First to notice is that, for each scenario, the efficiency changes with both H_2 and CO_2 injection variation are small (in the order of 1%). Furthermore, the efficiency always decreases with both CO_2 and H_2 injection, mainly for the following reasons: the Sabatier reaction and the electrolysis process have their own energy efficiency therefore, increasing the reactants flow rate gives more weight to these reaction efficiencies (reaction 2.15 and 2.8) in the overall energy efficiency of the process. Additionally, the injection of superfluous CO_2 only causes an energy penalty due to its cyclic separation and circulation.

As it can be seen on Figure 4.2, Scenario 1 has the highest system efficiency for all the H_2 amount injected. This is mainly because Scenarios 3 and 4 suffer for an energy penalty related to the CO_2 separation prior to the Sabatier reactor; in these scenarios all the CO_2 is separated before it can be injected, while in Scenario 1 only the unreacted CO_2 needs to be removed. Nevertheless, the energy advantages of Scenario 1 are counterbalanced by a heavier investment cost for the reactor which has to be sized according to the entire flow rather than by the only desired reactants flow.

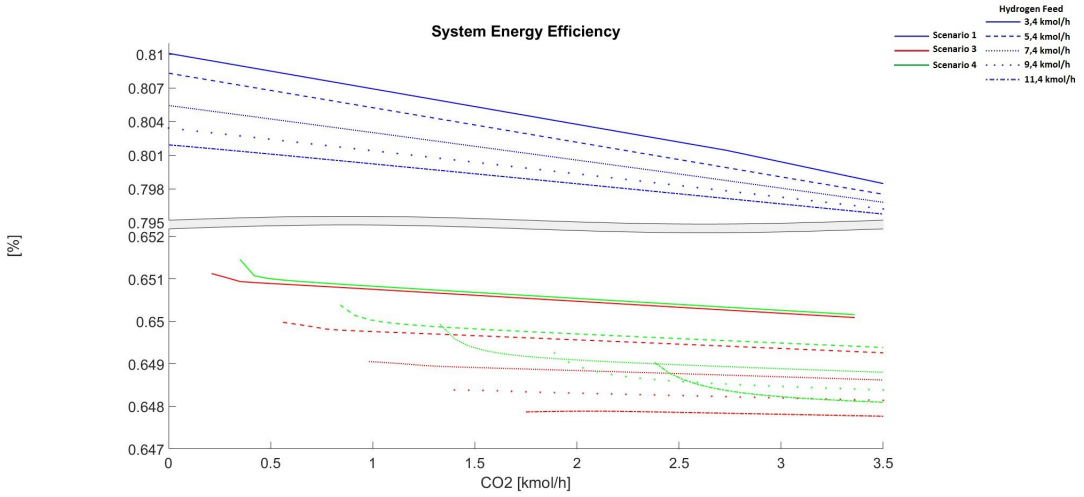

Figure 4.2: The sytem energy comparison for Scenario 1, 3 and 4 when H_2 is supplied by alkaline electrolyzer.

Figure 4.3 shows the exergy efficiency of Scenario 1, 3 and 4. The exergy efficiency resembles the system energy efficiency trends except for the trend related with the variation of H_2 feed which is reversed instead. Giving a quality-weight to the different forms of energy produced and consumed, more importance should be given to the biogas production, which increases with the H_2 feed. A similar trend will be also notable in the revenues, which like the exergy, gives a different weight to the energy streams by different prices. Remember, the reference temperature for the exergy content of the heat flows was taken to be the annual average temperature of Göteborg, which is 8°C. The slight difference in exergy for Scenario 3 and 4 is due to the hydrogen content in the biogas.

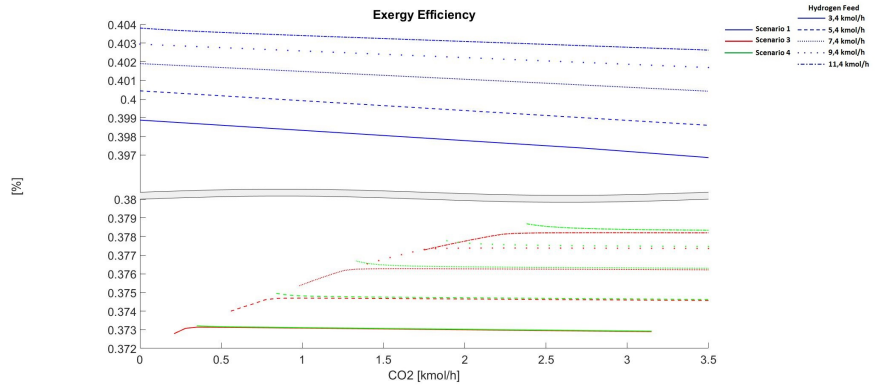

Figure 4.3: The exergy efficiency comparison for Scenario 1, 3 and 4 when H_2 is supplied by alkaline electrolyzer.

Figure 4.4 shows the cold gas efficiency for Scenario 1, 3 and 4. Remember, in

Scenario 2, CO_2 in the gas stream from the methanation reactor is made to be completely converted by injecting excess H_2. As expected, the cold gas efficiency of all the scenarios increases with increasing H_2 feed. The small difference (approximately 0,002) in the cold gas efficiency between different scenarios for the given amount of H_2 is due to the H_2 content remained in the biogas. Scenario 1 has the lowest amount of H_2 in the biogas because of the high conversion due to high concentration of CO_2 in the gas streams to the Sabatier reactor. The cold gas efficiency of the Scenario 3 increases gradually and then stabilizes, because of the removal of unconverted H_2 from the system; hence the cold gas efficiency increases with increasing CO_2 until H_2 is totally consumed.

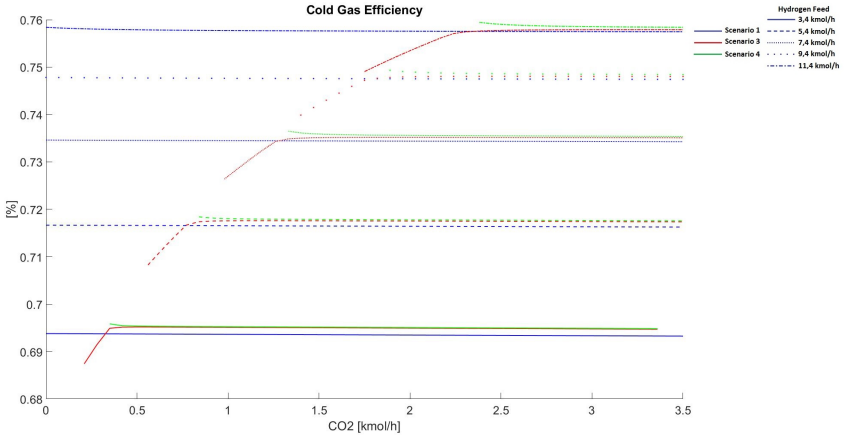

Figure 4.4: The cold gas efficiency comparison for Scenario 1, 3 and 4 when H_2 is supplied by alkaline electrolyzer.

Figure 4.5 shows the thermodynamic performance of Scenario 2. In this scenario, the aim was to completely convert CO_2, with the assumption that H_2 is abundantly available. This reduces the flexibility of the plant (the size of the gasification plant is limited by the H_2 availability) which can only operate within a short range of abundant hydrogen but, at the same time, it avoids the installation of a CO_2 separation unit.

All the graphs show an insignificant range of efficiency changes for the given range of H_2 feed. Note that only the cases where the gas quality boundary condition is met are shown on the all the graphs. Given the very short variation and the modelling accuracy, it is pointless to discuss their trends, however it is possible to state that the system energy efficiency, the cold gas efficiency and the exergy efficiency are respectively around 80%, 76% and 40%. It is interesting to notice that scenario 1 gives similar performances results when CO_2 is completely converted, as it could be expected: the main difference between these two scenarios is in the CO_2 removal which yet does not affect the system when all the CO_2 has been converted (when H_2 is abundantly supplied). It is good to remember that the H_2 recovered in the separation unit is then recycled (only the net H_2 supplied to the system is used in the performance evaluation).

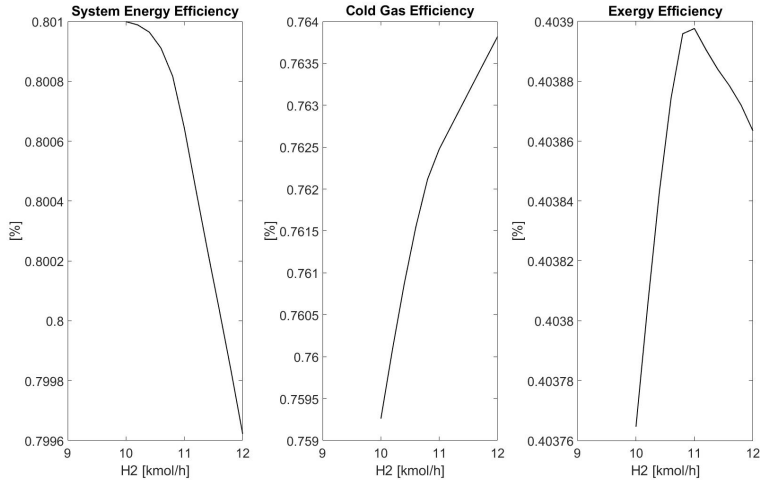

Figure 4.5: The thermodynamic performance of Scenario 2.

4.2.2 Efficiencies with PEM electrolyzer

Figure 4.6 shows the system energy efficiency for Scenario 1, 3 and 4 when H_2 is supplied by PEM electrolyzer. The system energy fall with the increasing amount of H_2 feed to the system, owing to the electric consumption by electrolyzer. The trends are similar to those discussed in the analogue chart for the alkaline electrolyzer both for what concerns CO_2 and H_2 feed and plant layouts, nevertheless the lines are all shifted down as expected when applying an electrolysis technology with lower efficiency.

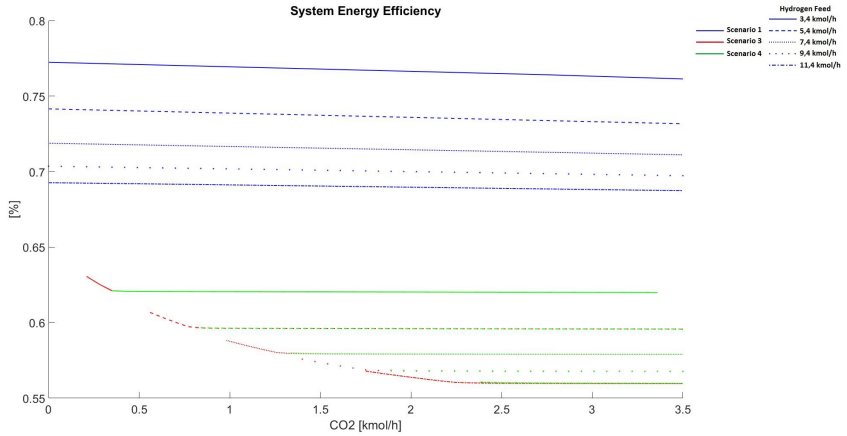

Figure 4.6: The system energy efficiency for Scenario 1, 3 and 4, when H_2 is supplied by PEM electrolyzer.

The exergy efficiency, applying PEM electrolizer, shows the same trends shown for the alkaline electrolyzer but with an overall drop of the performances, see Figure 4.7.

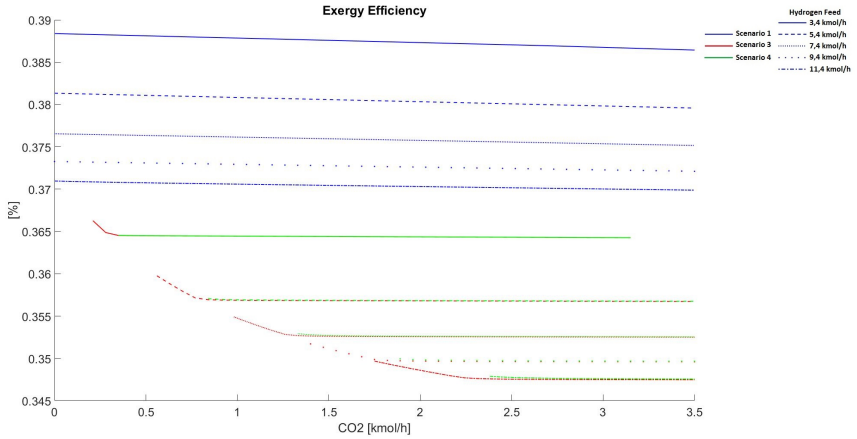

Figure 4.7: The exergy efficiency for Scenario 1, 3 and 4, when H_2 is supplied by PEM electrolyzer.

The cold gas efficiency doesn't vary with the electrosysis technology. This is validated by the graph in Figure 4.8 which is identical to its analogue for the alkaline electrolyzer.

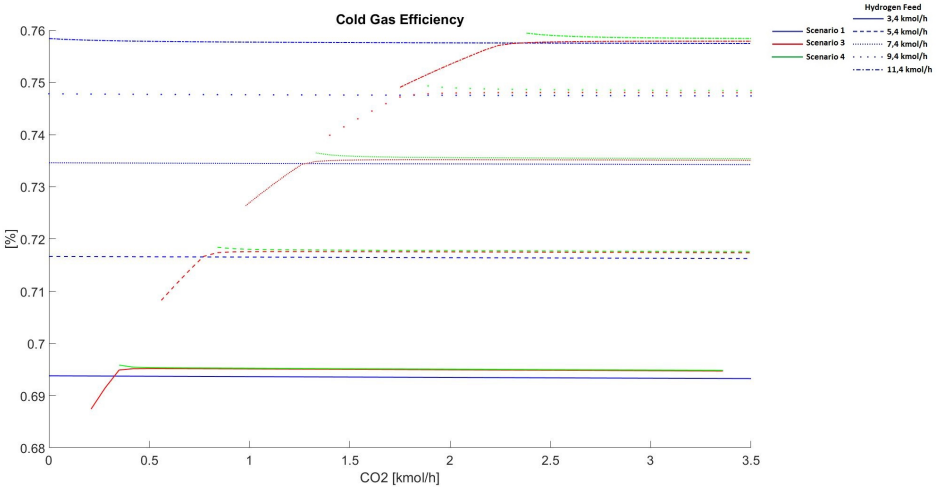

Figure 4.8: The cold gas efficiency for Scenario 1, 3 and 4, when H_2 is supplied by PEM electrolyzer.

Figure 4.9 depicts the thermodynamic performance of Scenario 2 when H_2 is supplied by the PEM electrolyzer. Again, the little variation of efficiency makes little sense to comment the sensitivity analysis trend, however we can notice the severe energy efficiency drop that characterizes this technology compared to the other scenarios. This is due to the H_2 feed that in this scenario always have to always be and obviously the energy required to provide the H_2 feed is directly dependent on the electrolysis technology.

The exergy efficiency of the Scenario 2 decreases with increasing H_2, it is due to the fact that electric energy demand for the PEM electrolyzer is growing faster than

other parameters of equation 3.5, leading to exergy efficiency reduction.

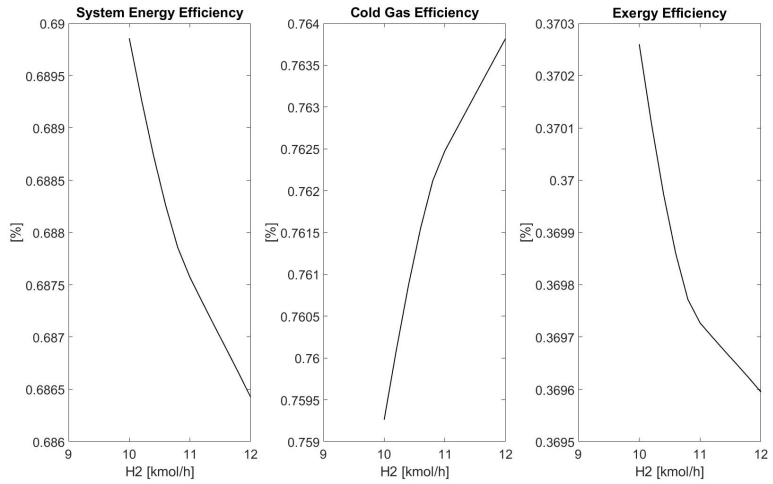

Figure 4.9: Thermodynamic performance for Scenario 2 when H_2 is provided by a PEM electrolyzer.

4.3 Economic performance of scenarios

The recycling of CO_2 and variation of H_2 feed affects the size of the Sabatier reactor (for a given biomass feed). Variation of reactor size would then have an economic penalty (investment and logistic costs) on the system, therefore it is essential to find out how reactor size changes with the gas flow. Figure 4.10 and 4.11 show the size change of the Sabatier reactor for the scenarios (Scenario 1 and 2) where the outlet gas stream of methanator is directly sent to the Sabatier and for the scenarios (Scenario 3 and 4) when CO_2 is separated and sent to the Sabatier.

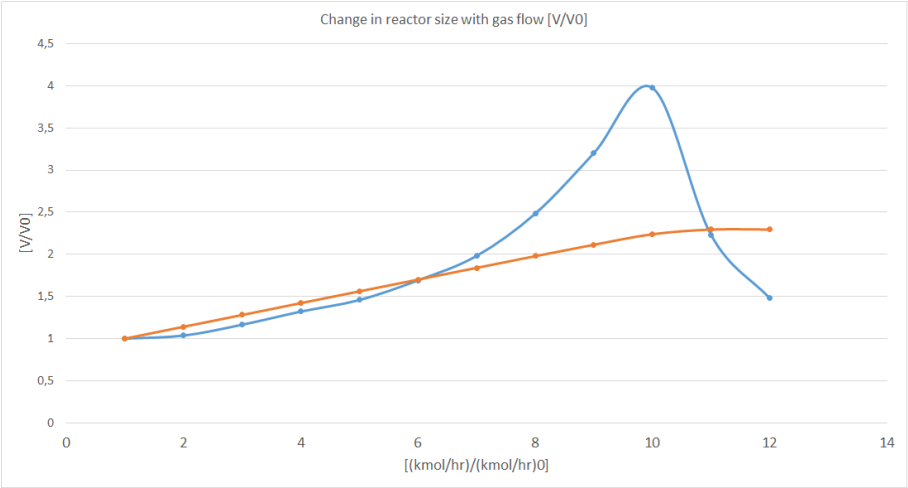

Figure 4.10: Change in size with gas flow for the Sabatier reactor, when gas stream of CO2+CH4 is, without separation of CO_2, sent to the Sabatier reactor (Scenario 1 and 2). The blue and orange graphs show the proportional variation of reactor size and biogas production with regards to a given reference, respectively.

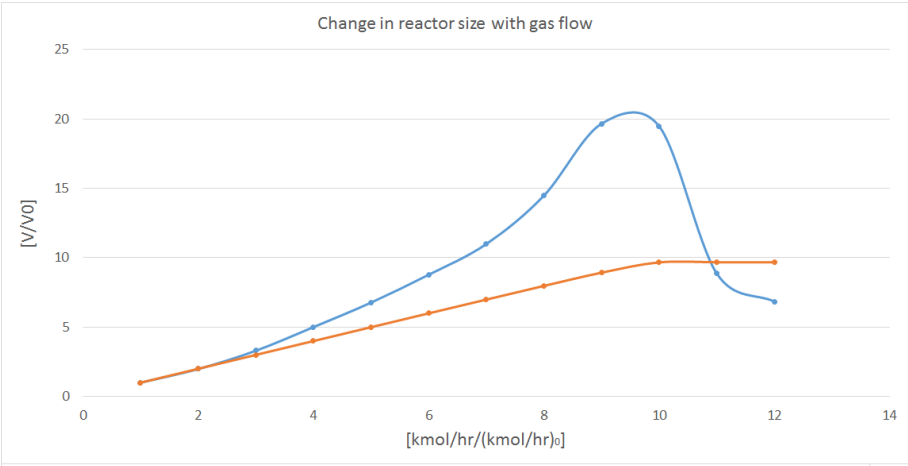

Figure 4.11: Change in size with flow for the Sabatier reactor, when CO_2 is separated from CO2+CH4 stream and injected to the Sabatier reactor (Scenario 3 and 4). The blue and orange graphs show the proportional variation of reactor size and biogas production with regards to a given reference, respectively.

The graphs refers to a fixed amount of CO_2 injected and shows the reactor size (blue) and the methane produced (orange) relative variation versus the relative variation of H_2 injected. It can be noticed that the size of the reactor decreases at the extremities of the H_2 injection interval, and this could have been expected since they represent the cases where either CO_2 (left extremity) or H_2 (right extremity) is overabundant, boosting the reaction driving force. In order to obtain the same reaction extent rate with stochiometric inputs, the driving force of the reaction has to be enhanced with the volume of the reactor itself. Still, for a fixed amount of

CO_2, the minimum reactor size correspond to the minimum H_2 feed, moreover, a surplus of H_2 doesn't contribute to a higher methane production once that the CO_2 has been completely converted, but can help the velocity of the reaction decreasing the reactor size; indeed an excess of H_2 could be advantageous under a reactor size-versus-production prospective. Note that even if for scenario 3 and 4 the relative size increase peaks 20 times as big while for scenario 1 and 2 only 4 times as big, the initial size of the reactor (to which all is scaled and referred) is much bigger (more than 7 times bigger) for scenario 1 and 2 than in scenario 3 and 4. Furthermore, while for scenarios 3 and 4 the reactor dimension is not affected by the size of the plant (it is only affected by the CO_2 and H_2 feed streams which can both be dosed independently), for scenario 1 and 2 the reactor size is heavily affected by the plant size itself, since all the gas is directly injected in the Sabatier unit without prior separation.

4.3.1 Profit with alkaline electrolyzer

Figure 4.12 and 4.13 shows the operational profits and a biogas production, respectively, for Scenario 1, 3 and 4 when H_2 is supplied by alkaline electrolyzer. The operational profits is positive, meaning that the plant could payback its investment cost. The two figures illustrate that both operational profits and the biogas production for all the scenarios sensibly increase with increasing H_2 feeding.

Scenarios 3 and 4 are similar even if scenario 3 has a higher flexibility (wider operational range) due to the H_2 removal unit. Scenario 1 is always slightly more economically advantageous regardless of the H_2 or CO_2 supply, although it is good to remember that this values refers to operational income, while Scenario 1 is economically penalized by a higher investment costs, which is due to the bigger reactor required to handle the relatively higher incoming flow . The trends are linear except for some kinks which represent the biogas composition type thresholds and the consequent devaluation of fuel type according to the Wobbe Index.

It is seen in Figure 4.13 that Scenario 1 starts producing biogas right away with H_2 injection; it is because of sufficient CO_2 that is already present in the incoming gas stream from the methanator (see also Figure 3.6). Nevertheless, the biogas production for all the scenarios becomes equal as more and more CO_2 is fed to Scenario 3 and 4.

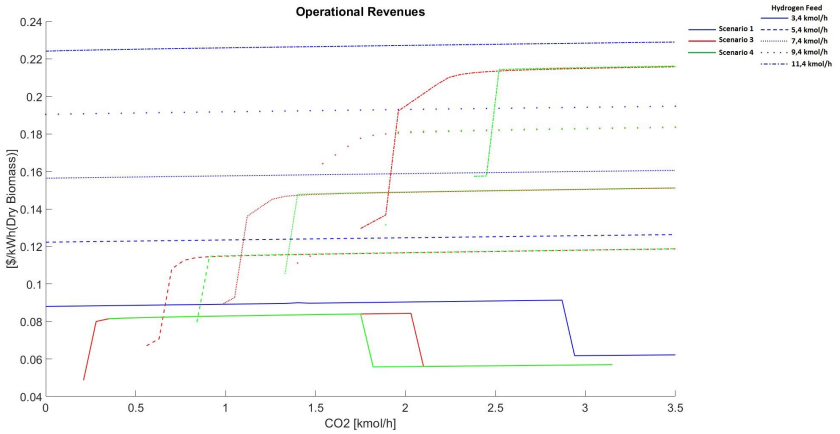

Figure 4.12: Operational profits for Scenario 1, 3 and 4 when H_2 is supplied by alkaline electrolyzer.

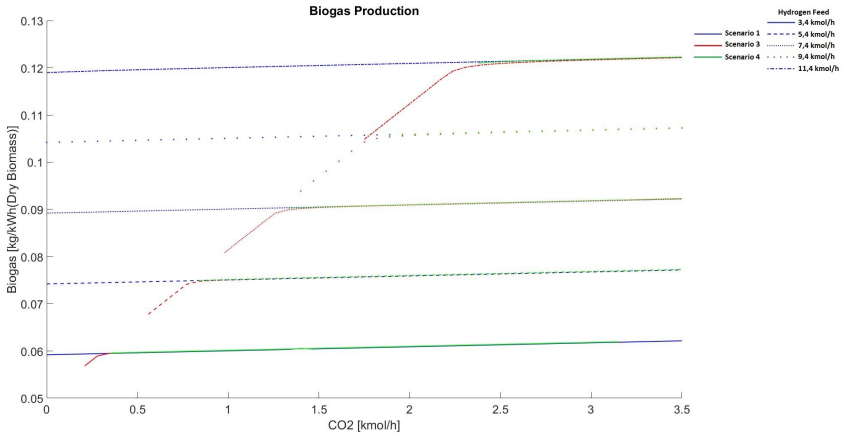

Figure 4.13: Biogas production for Scenario 1, 3 and 4 when H_2 is supplied by alkaline electrolyzer.

Figure 4.14 shows the operational cost and biogas production in Scenario 2 while varying H_2 injection from the alkaline electrolyzer. The graph on the left in the figure shows that as H_2 increases, operational profit increases and then falls abruptly, indicating that the production of type-B starts; in the range of H_2 feed between 10,3 and 11,6 instead, the trend follows the biogas production. The initial drop of biogas production is due to conversion of CO_2, since the water formed in the conversion is condensed out, and given that the molecule of CO_2 is heavier than that of CH_4, the gas richer in CO_2 is thus heavier. But after that the CO_2 is completely converted, the extra H_2 remains in the biogas increasing its weight(linearly).

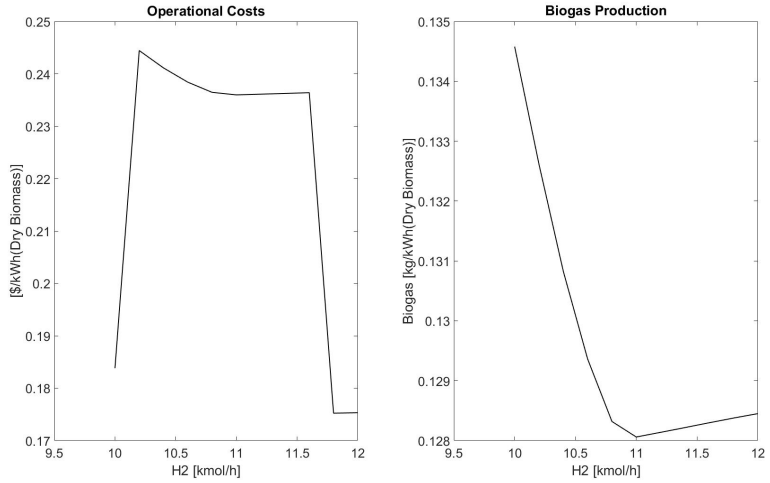

Figure 4.14: Economic performance of Scenario 2 when H_2 is supplied by an alkaline electrolyzer.

4.3.2 Profit with PEM electrolyzer

It can be easily verified that the electrolysis technology does not affect the biogas production, Figure 4.16 and the graph on the right side of Figure 4.17 are identical to their analogous for the alkaline elctrolyzer. Moreover, from Figure 4.15 and the graph on the left side in Figure 4.17 it can be estimated the burden of the lower efficiency(see Table 2.3) of the PEM electrolyzer on the revenues.

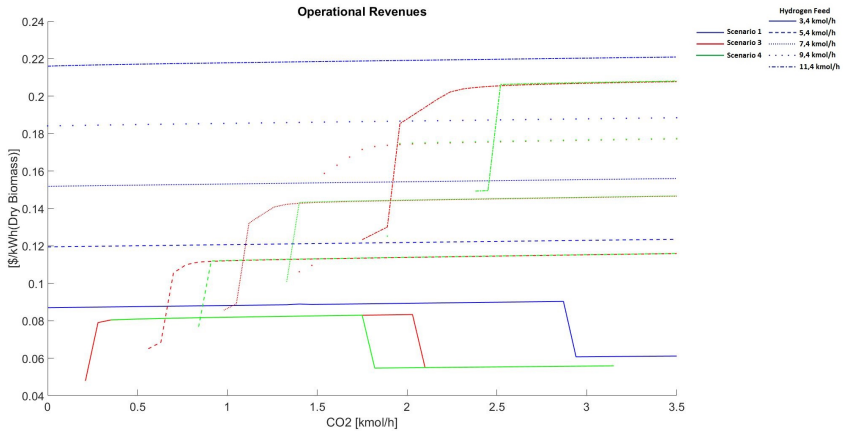

Figure 4.15: Operational profits from Scenario 1, 3 and 4 when H_2 is supplied by a PEM elctrolyzer.

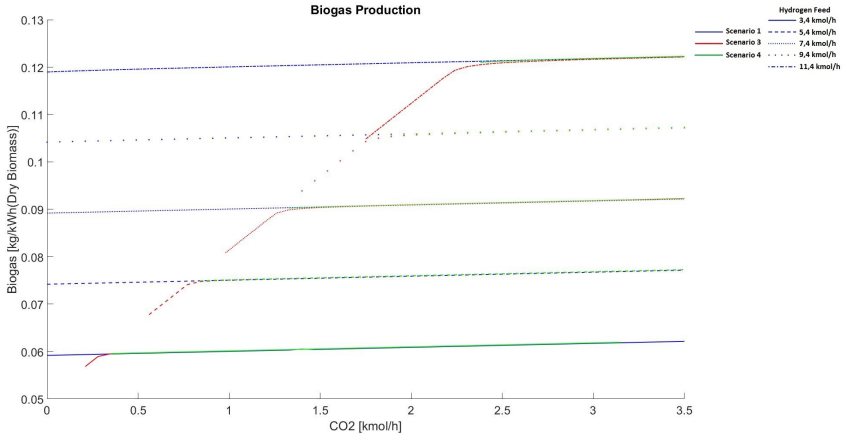

Figure 4.16: Biogas production from Scenario 1, 3 and 4 when H_2 is supplied by a PEM electrolyzer.

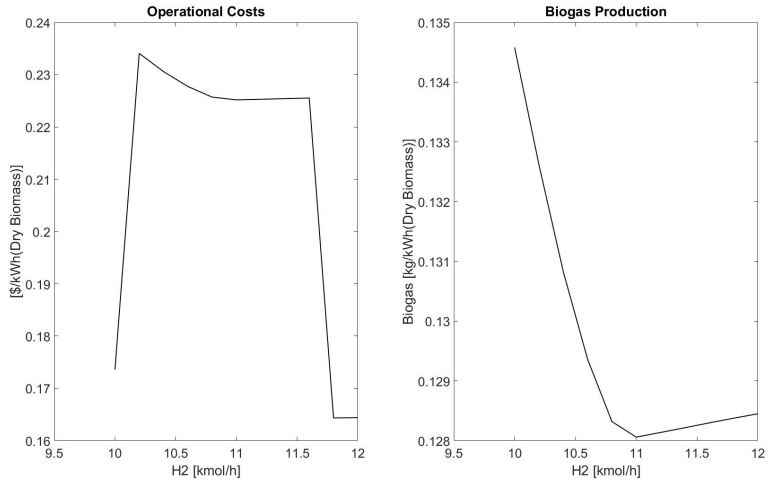

Figure 4.17: Economic performance of Scenario 2 with PEM electrolyzer.

4.4 Sensitivity to performance indicators

The integration of P2G technologies to the gasification system increases the assimilation of intermittent electricity into the energy system. The genuine performance of these technologies depends upon the degree to which the system can harness the intermittent electricity. The consideration to the timely imbalance between the electric load and intermittent energy generation (the so-called duck curves) can yield an inner sight as to how the system has to operate if the full potential of the intermittent energy has to be utilized. The duck curves can provide the operational path of the system and help to chose the type of electrolyzer technology that is fast enough to respond to the fluctuation of the path. Therefore it is important to investigate the system performance versus the variation of the available intermittent electricity.

The electric price of $0,024/kWh has been used in the calculation of operational costs. This price was 50% of the average electric price sold to the industry customers. The idea was that it could give the average off-peak electricity prices which could lie in the range of 0-$0,048/kWh. Even with that assumption, the operational profits in all the scenarios are positive (meaning that the revenue is bigger than the costs). However, the positive operational cost determined according to section 3.3.2 says not that much about the real economic performance of the plant. In order to get the genuine economic performance, the consideration to the total operational costs which included investment, labour and engineering cost have to be determined to asses the economic feasibility of the plant. The biogas cost used in the calculation of operational profits represent the most optimistic scenarios because costs related to distributions and logistics are neglected. Generally, a complete and decisive economic assessment of the plant require a rigorous approach where the energy prices are determined with the consideration to energy market based on different energy policies.

5
Conclusion

The overall picture given by the modelling results says that an operational profit could be achievable in each scenario. The energy efficiency always seems to drop with the hydrogen feed, but this trend is reversed for the economic incomes and for the biogas production (like in a balance between quality and quantity).
As expected, scenarios which requires (on a first hypothesis) higher investment costs also lead to higher operational profits. Scenario 2, however, achieve both high profits and low investment costs, but is extremely penalized by the operational flexibility: the size of the Sabatier reactor and the hydrogen feed are imposed by the size of the plant.

Both energy and cold gas efficiency figures are comparable with those of an indirect gasifier, which makes a further capital cost investigation reasonable and interesting.

Neither the size of the Sabatier reactor and the methane conversion vary linearly with its inlet flow, which means that a cost optimization should be performed according to the plant and the unit sizes.

The results of the two investigated electrolysis technologies shows the weight of the electrolysis energy efficiency on the overall process efficiency. This allow to determine the range of operational boundaries (such as energy peaks frequency, duration, or intensity and electricity prices) which better fits each technology. Other plant layouts, different technologies and materials utilization could not have been investigated for a shortage of time, yet this work is a solid basis for them.

5.1 Future Works

In the following, the future works which could be done based on this work are presented.

- The scaling up investigation of the plant and the investment cost analysis: this study takes into account the operational performance (both energy and economic) of the plant, however, for this model the size of the plant does not affect these performance and has not been taken into account for the economic analysis. Several parameters, such as investment costs, heat and pressure losses and components service life are not linearly dependent with the plant size. Hence a further analysis taking into account these parameters could be carried based on this work.

- Perform the kinetic modeling of the direct gasification process: this study bases the gasification process modelling on the experimental data of the available literature, but it is not sensitive to the operational parameters (such as pressure, temperature and feedstock particles shape). In order not to be restricted to the used operational parameters a deeper study on the kinetics of the direct gasification process is necessary. After that, a sensitivity analysis of the operational parameters of the gasification unit could be integrated to this work.
- Investigate the model performance with regards to the electricity peaks' frequency intensity, and duration: one of the aims of this work is to asses the advantages of electrolysis and direct gasification integration, especially when electrolysis is driven by peak (therefore cheaper) electricity. The nature of these peaks is unpredictable. For this reason, it is important to choose the electrolysis technology taking into account also dynamic parameters (not used in this study) such as responsiveness, reliability and sensitivity to current's intensity or voltage that better fits the electrical grid load fluctuations. Hence, a further analysis on the different electrolysis technologies and their dynamic performance could support our work in defining the most advantageous integration options.
- Evaluate the environmental impact assessment of the scenarios: aiming to a sustainable development, this work could be used to future studies to asses and compare different energy pathways according to fossil-fuels replacement, emission reduction and renewable energies integration (since smoothing out peak loads would help in stabilizing the grid, allowing the integration of further intermittent energy production).
- In-depth plant design (heat exchanger networks, reactors' size, logistics, piping etc: although a conceptual scheme of the plant layout is provided in this work, the actual layout requires a further analysis. The heat recovery, for example, has been calculated in order to achieve the maximum energy recovery (MER) for a minimum temperature difference assumed equal to 10K, however, the MER network could be not the economically most convenient choice and the minimum temperature difference should also be part of a more specific techno-economical analysis. Other techno-economical aspects regarding the design of each specific device are also topics for a future study based on this work.

Bibliography

[1] H. Hermann, R. Reinhard, and R. Karl, "Gas cleaning for synthesis applications," *ThermalNet*, p. 269–294, 2007.

[2] P. Basu, *Biomass Gasification and Pyrolysis: Practical Design and Theory*. Kidlington, Oxford,OX5 1GB, UK: Elsevier, 2010.

[3] M. Antonio, C. Simeone, and M. Dino, "Biomass gasification technology: The state of the art overview," *Journal of Energy Chemistry*, vol. 10-25, pp. 851–860, 2016.

[4] S. Heyne, H. Thunman, and S. Harvey, "Exergy-based comparison of indirect and direct biomass gasification technologies within the framework of bio-sng production," *Biomass Conv. Bioref.*, vol. 337-352, 2013.

[5] E. Sette, D. Pallarès, and F. Johnsson, "Influence of bulk solids cross-flow on lateral mixing of fuel in dual fluidized beds," *Fuel Processing Technology*, vol. 140, pp. 245–251, 2015.

[6] R. Reinhard, H. Jitka, and H. Hermann, "Biomass gasification for synthesis gas production and applications of the syngas," *Journal of Energy Chemistry*, vol. 10-25, pp. 851–860, 2013.

[7] A. Albert, *Large-Scale Production and Use of Biomethane*. PhD thesis, CHALMERS UNIVERSITY OF TECHNOLOGY, 2016.

[8] "SGC-Svenskt Gastekniskt Center AB." `http://www.sgc.se/ckfinder/userfiles/files/demo029.pdf`. Accessed: 2017-03-26.

[9] I. Hannula and E. Kurkela, "A parametric modelling study for pressurised steam/O_2-blown fluidised-bed gasification of wood with catalytic reforming," *BIOMASS AND BIOENERGY*, vol. 38, pp. 58–67, 2012.

[10] A. Alamia, S. Henrik, and T. Henrik, "Design of an integrated dryer and conveyor belt for woody biofuels," *BIOMASS AND BIOENERGY*, vol. 77, pp. 92–109, 2010.

[11] S. Heyne and H. Simon, "Production of synthetic natural gas from biomass-process integrated drying," *Proceedings of ECOS 2009*, 2009.

[12] K. Priyanka and T. Rakesh, "Advanced simulation of biomass gasification in a fluidized bed reactor using aspen plus," *Renewable Energy*, vol. 629-636, 2017.

[13] A. Ahmed, A. Salmiaton, T. Choong, and W. Azlina, "Review of kinetics and equilibrium concepts for biomass tar modeling by using aspen plus," *Renewable and Sustainable Energy Reviews*, vol. 52, pp. 1623–1644, 2015.

[14] P. Carolina, "Modelling of tar formation and evolution for biomass gasification: A review," *Applied Energy*, vol. 111, p. 129–141, 2013.

[15] "Air separation." `https://en.wikipedia.org/wiki/Air_separation`. Accessed: 2017-04-06.

[16] T. Banaszkiewicz, M. Chorowski, and W. Gizicki, "Comparative analysis of cryogenic and ptsa technologies for systems of oxygen production," *American Institute of Physics*, 2014.

[17] J. Don-Stevens, "Hot gas conditioning: Recent progress with larger-scale biomass gasification systems," *National Renewable energy Laboratory*, p. 269–294, August 2001.

[18] W. Xiaoxing, M. Xiaoliang, X. Xiaochun, S. Lu, and S. Chunshun, "Mesoporous-molecular-sieve-supported polymer sorbents for removing h2s from hydrogen gas streams," *Springer Nature*, vol. 49, April 2008.

[19] X. Hong-Jian, Z. Cheng-Fang, and Z. Zhi-Sheng, "Selective H_2S removal by non-aqueous methyldiethanolamine solutions in an experimental apparatus," *Ind. Eng. Chem. Res.*, vol. 41, pp. 2953–2956, 2002.

[20] Q. Zhi, X. Lian-Bin, L. Zhen-Hu, L. Hua, and G. Kai, "Selective absorption of H_2S from a gas mixture with CO_2 by aqueous n-methyldiethanolamine in a rotating packed bed," *Ind. Eng. Chem. Res.*, vol. 49, p. 6196–6203, 2010.

[21] "The Capture and Sequestration of Carbon Dioxide." `http://www.esru.strath.ac.uk/EandE/Web_sites/02-03/carbon_sequestration/Carbon%20Sequestration-423.htm`. Accessed: 2017-05-07.

[22] J. POLASEK and A. BULLIN, "Selecting amines for sweetening units," tech. rep.

[23] K. . Jan, J. Tilman, M. Serge, and Biollaz, "Production of synthetic natural gas (SNG) from coal and dry biomass – a technology review from 1950 to 2009," *Fuel*, vol. 89, p. 1763–1783, 2010.

[24] D. Schelereth, *Kinetic and Reactor Modeling for the Methanation of Carbon Dioxide*. PhD thesis, Technischen Universität Munchen, 2015.

[25] A. Rehmat and S. Sarabjit, "Selective methanation of carbon monoxide," *Ind. Eng. Chem. Prod. Res. Develop*, vol. 9, 1970.

[26] "HALDOR TROPSOE." `http://www.topsoe.com/industries/bio-fuels`. Accessed: 2017-04-07.

[27] G. P. S. Plant, "Practical experience gained during the first twenty years of operation of the great plains gasification plant and implications for future projects," tech. rep., U.S. Department of Energy, April 2006.

[28] H. Bijan, R. John, B. Xiaota, and A. Mahecha-Botero, "Kinetic model of steam gasification of biomass in a bubbling fluidized bed reactor," *Energy Fuels*, vol. 31, pp. 1702–1711, 2017.

[29] J. Liu, D. Cui, J. Yu, F. Su, and G. Xu, "Performance characteristics of fluidized bed syngas methanation over $Ni - Mg/Al_2O_3$ catalyst," *Chinese Journal of Chemical Engineering*, vol. 23, p. 86–92, 2015.

[30] X. Yana, Y. Liu, B. Zhao, Z. Wang, Y. Wang, and C. Liu, "Methanation over Ni/SiO_2: Effect of the catalyst preparation methodologies," *International Journal of Hydrogen Energy*, vol. 38, p. 2283–2291, 2013.

[31] T. Johannesson, "Implementation of electrofuel production at a biogas plant, Case study at Borås Energy and Miljö," Master's thesis, Chalmers University of Technology, Göteborg, Sweden, 2016.

[32] J. Christian, H. Kyle, W. Dennis, and R. Subir, "Compact and lightweight sabatier reactor for carbon dioxide reduction," *American Institute of Aeronautics and Astronautics*.

[33] L. Jürgensen, E. Augustine, , E. Augustine, and J. Holm-Nielsen, "Dynamic biogas upgrading based on the sabatier process: Thermodynamic and dynamic process," *Bioresources Technology*, vol. 178, pp. 323–329, 2015.

[34] B. Kriston, H. Jianli, Z. H. Zhub, and J. Robert, "Methanation of carbon dioxide by hydrogen reduction using the sabatier process in microchannel reactors," *Chemical Engineering Science*, vol. 62, pp. 1161–1170, 2006.

[35] P. Luis, "Use of monoethanolamine (MEA) for CO_2 capture in a global scenario: Consequences and alternatives," *Desalination*, vol. 380, pp. 93–99, 2016.

[36] A. C. Yeh and B. Hsunling, "Comparison of ammonia and monoethanolamine solvents to reduce CO_2 greenhouse gas emission," *The Science of the Total Environment*, vol. 228, pp. 121–133, 1999.

[37] Y. Hongqun, X. Zhenge, F. Maohong, G. Rajender, B. Rachid, E. Alan, and W. Ian, "Progress in carbon dioxide separation and capture: A review," *Journal of Environmental Sciences*, vol. 20, pp. 14–27, 2008.

[38] I. Jose, D. M. Gomez, G. Nicolas, and G. Jessica, "CO_2 absorbing capacity of mea," *Journal of Chemistry*, vol. 337-352, p. 7, 2015.

[39] "CO2 scrubbing process overview." `http://www.rwe.com/web/cms/en/2734/rwe/innovation/power-generation/fossil-fired-power-plants/co2-scrubbing/`. Accessed: 2017-03-21.

[40] S. W. E. Agency, "Introduction to the production of biomethane from biogas - a guide for ENGLAND and WALES (UK)," tech. rep., INTELLIGENTENERGY.

[41] A. Alamia, A. Larsson, C. Breitholtz, and H. Thunman, "Impact of choice of co2 separation technology on thermo-economic performance of bio-sng production processes," *International Journal of Energy Research*, vol. 38, 2013.

[42] S. Papadokonstantakis. private communication, 2017.

[43] "PSA Technology: Beyond Hydrogen Purification." `http://www.chemengonline.com/psa-technology-beyond-hydrogen-purification/?printmode=1`. Accessed: 2017-03-30.

[44] A. Carlos, "Advances in pressure swing adsorption for gas separation," *HINDAWI*, p. 13, 2012.

[45] B. Ana-Maria, F. Daniel, B. Stefano, and D. Tina, "A multiscale study of MOFs as adsorbents in H_2S PSA purification," *Eng. Chem.*, vol. 52, pp. 9946–9957, 2013.

[46] A. Mivechian and M. Pakizeh, "Hydrogen recovery from tehran refinery off-gas using pressure swing adsorption, gas absorption and membrane separation technologies: Simulation and economic evaluation," *Korean J. Chem. Eng*, vol. 30, pp. 937–948, 2013.

[47] P. David and P. M. K., "Techno-economic implications of the electrolyser technology and size for power-to-gas systems," *International Journal of Hydrogen Energy*, vol. 41, p. 3748–3761, 2016.

[48] C. Stephan and M. Pierluigi, "Integrated modeling and assessment of the operational impact of power-to-gas (p2g) on electrical and gas transmission networks," *IEEE*, vol. 6, pp. 323–329, 2015.

[49] "Nel A – Atmospheric Electrolyser." http://nelhydrogen.com/product/electrolyser/. Accessed: 2017-03-27.

[50] "Proton on site." http://www.protononsite.com/products/m-series. Accessed: 2017-03-27.

[51] B. Selma, T. Maria, G. Maria, and H. Julia, "Electrofuels for the transport sector: a review of production costs," *Not yet published*, 2016.

[52] Mathiesen, V. Brian, S. Iva, Ridjan, Connolly, David, Nielsen, M. Pagh, V. Hendriksen, Peter, B. Mogensen, Mogens, H. Jensen, Søren, D. Ebbesen, and Sune, "Technology data for high temperature solid oxide electrolyser cells, alkali and PEM electrolysers," tech. rep., Aalborg Universitet, 2017.

[53] "Elproduktion." https://www.energiforetagen.se/sa-fungerar-det/el/produktion/. Accessed: 2017-04-25.

[54] "Wind power in Sweden." https://en.wikipedia.org/wiki/Wind_power_in_Sweden. Accessed: 2017-04-25.

[55] "Energymyndighten, Produktion och utbyggnad." http://www.energimyndigheten.se/fornybart/vindkraft/marknadsstatistik/. Accessed: 2017-04-25.

[56] "Solkraft." https://www.energiforetagen.se/sa-fungerar-det/el/produktion/solkraft/. Accessed: 2017-04-25.

[57] "Energimyndigheten, Bättre förutsättningar för solceller på villataket." http://www.mynewsdesk.com/se/statens_energimyndighet__stem/pressreleases/baettre-foerutsaettningar-foer-solceller-paa-villataket-1475307. Accessed: 2017-04-25.

[58] M. Guilnaz, L. Hailong, T. Eva, and D. Erik, "Evaluation of different biomass gasification modeling approaches for fluidized bed gasifiers," *Biomass and Bioenergy*, vol. 91, p. 69–82, 2016.

[59] B. Mehrdokht and M. Nader, "Simulation of biomassgasification in fluidizedbed reactor using aspenplus," *BIOMASS AND BIOENERGY*, vol. 32, pp. 1245–1254, 2008.

[60] A. Technology, "Aspen plus 12.1 unit operation models," tech. rep., Aspen Technology, Inc., June 2003.

[61] A. Alamia, A. Larsson, C. Breitholtz, and H. Thunman, "Performance of large-scale biomass gasifiers in a biorefinery, a state-of-the art-reference," *WILEY VCH*, 2016.

[62] M. Arvidsson, *Assesing the Integration of Biomass Gasification-Based Production of Chemicals- Case Study of an Oxo Synthesis Plant.* Licentiate thesis, Chalmers University of Technology, Göteborg, Sweden, 2014.

[63] "Normal årsmedeltemperatur." http://www.smhi.se/klimatdata/meteorologi/temperatur/normal-arsmedeltemperatur-1.3973. Accessed: 2017-05-07.

[64] "APPENDIX 1. STANDARD CHEMICAL EXERGY, by Szargut J., Egzergia. Poradnik obliczania I stosowania, Widawnictwo Politechniki Shlaskej, Gliwice

2007.” http://web.mit.edu/2.813/www/readings/APPENDIX.pdf. Accessed: 2017-05-07.

[65] “Priser på el för industrikunder 2007–.” http://www.scb.se/hitta-statistik/statistik-efter-amne/energi/prisutvecklingen-inom-energiomradet/energipriser-pa-naturgas-och-el/pong/tabell-och-diagram/genomsnittspriser-per-halvar-2007/priser-pa-el-for-industrikunder-2007/. Accessed: 2017-05-02.

[66] “Vad kostar det att köra på biogas?.” https://www.eon.se/privat/for-bilen/koera-pa-biogas/vad-kostar-det.html. Accessed: 2017-05-02.

[67] “ecoinvent.” http://www.ecoinvent.org/database/database.html. Accessed: 2017-05-10.

[68] “Sjunkande priser på trädbränsle och torv.” http://www.energimyndigheten.se/nyhetsarkiv/2016/sjunkande-priser-pa-tradbransle-och-torv2/. Accessed: 2017-05-02.

[69] “Heat of combustion.” https://en.wikipedia.org/wiki/Heat_of_combustion. Accessed: 2017-05-10.

A

LHHW model, Standard Exergy and Biomass analysis

Equation A.1 is the kinetic model for the Sabatier process developed by Schlereth [24]. Schlereth investigated the robustness of the model by comparing the model-produced data with the experimental one, while Ni-alumina catalyst was used as the catalyst. The equation applies under the circumstance that formly functional group (HCO-X) is formed during the process.

$$r = k\frac{p_{H_2}^{0,5}p_{CO_2}^{0,5}(1-\frac{p_{CH_4}p_{H_2}^2}{p_{H_2}^4 p_{CO_2}K_{eq}})}{(1+K_{OH}\frac{p_{H_2O}}{p_{H_2}^{0,5}}+K_{H_2}p_{H_2}^{0,5}+K_{mix}p_{CO_2}^{0,5})^2} \tag{A.1}$$

where r is the rate of the reaction, k is the kinetic factor, K_{eq} is the equilibrium constant, p_i is the partial pressure of component i, K_j is the adsorption constants of species (H_2, OH and their mixture). In Table A.1 and A.2 the adsorption and equilibrium constants used in the LHHW are given [24].

Table A.1: Equilibrium and adsorption constants for LHHW model [24].

Constant	A	B	C	Unit
$\ln K_{OH}$	-1,595	-2694	-	$Pa^{-0,5}$
$\ln K_{H2}$	-7,921	746	-	$Pa^{-0,5}$
$\ln K_{mix}$	-8,051	1203	-	$Pa^{-0,5}$
$\ln K_{eq}$	-18,106	19087	-3,998	$Pa^{-0,2}$

Table A.2: Activation energy and kinetic factor values for LHHW model [24].

k ($\frac{kJ}{PaKg_{cat}s}$)	E ($\frac{kJ}{mol}$)
6,0710*10	86,5

.

The activation energy, 86,5 $\frac{kJ}{mol}$, was proposed by Johannesson [31] because the model data with this activation energy was consistent with the experimental provided in by Schle [24]. The activation energy provided by Schlereth [24] was 77,5 $\frac{kJ}{mol}$.

Table A.3: Standard chemical exergy and molar mass of substances. (at T= 298.15K, p = 101.325 kPa) [64].

Substance	**Name**	**Molecular Mass (kg/kmol)**	**Standard chemical exergy (kJ/mol)**
C	Carbon (graphite)	12,01	409,07
CH_4	Methane	16,04	831,2
CO_2	Carbon dioxide	44,01	19,48
H_2	Hydrogen	2,02	236,09
H_2O	Water (gas form)	18,02	9,5
N_2	Nitrogen	28,01	0,71
O_2	Oxygen	31,99	3,97
S	Sulphur	32,064	609,6

Table A.4: The proximal analysis of the forest residues used used in the experiment [9].

Proximal analysis of the forest residues (w-%)	
Fixed Carbon	20,6
Volatile matter	76,8
Ash	2,6
Moisture	10,4

Table A.5: The ultimate analysis of the forest residues [9].

Element	Composition [w-%]
C	0,513
H	0,061
O	0,39
S	0,0005
N	0,005
ASH	0,026

B

Description of acronyms (for dryer, methanator and gasfier)

Table B.1: Description of acronyms for the components and streams in for the drying flowsheet.

Streams acronym	**Description**	**Components acronym**	**Description**
AIR	Atmospheric air	AIRHEAT	Air heater
HOTAIR	Heated air	AIRDRYER	Reactor to dry the biomass
DRYEROUT	Partially dried biomass together with vapor (air + water)	MOISTSEP	Separates the vapor from biomass
HUMIDAIR	Water vapor and air	AIRCOOL	Cool down the disposed air
AIROUT	Cooled water vapor and air to be disposed	DRYERi for i = 1,2	Dry the biomass at different level
BIOMASS1	Partially dried biomass	FLASHi for i = 1,2	Separates vapor from the biomass
MIXi for i = 1,2	Mixture of water vapor and partially dried biomass	INT-HEi for i = 1,2	Heat up the vapor
BIOMASS2	Further dried biomass	HEi for i = 1,2	Heat up the vapor
DRYB	Dry biomass	HEAT-L-i for i =1, 2	Cool down the vapor
MOISTi for i = 1,2	Moisture from biomass	VALVEi for i = 1,2	Split the vapor into different streams
STREAM-i for i = 1,2...12	Water vapor bieng transported therough different components	FANi for i = 1,2	Fans that blow the vapor
AIRIN	Air being blown in in the dryer at the next stage	BED-MIXi for i = 1,2	Mix vapor from biomass and steam
MOISTOUTi for i=1,2	Water vapor being disposed	EVACMIX	Mix inlet air with vapor
EVAC	Mixture of air and vapor	MOISTCON	Cools the mixture down

Table B.2: Variables with their corresponding values as they are used for the simulation of biomass drying.

Variables	**Value**	**Variables**	**Value**
AIR at 1 atm and 25°C, flow [kg/hr]	1	HEAT-L-1heaT duty [W]	-100
AIRHEAT temperature [°C]	110	HE1 temperature [°C]	155
WETBIO at 1 atm and 25°C, flow [kg/hr]	167	INT-HE1 heat duty [W]	500000
AIRDRYER temperature [°C]	90	DRYER2 temperature [°C]	117
MOISTSEP, FLASH1,2 vapor fraction out	1	HEAT-L-2 heat duty	-100
AIRCOOL temperature [°C]	50	HE2 temperature [°C]	130
DRYER1 temperature [°C]	101,25	INT-HE2 heat duty [W]	500000
FAN1,2 isentropic efficiency	0,75	INT-HE2 pressure drop (bar)	-0,003
FAN1,2 discharge pressure (bar)	1,03	VALVE1,2 flow of MOISOUT1,3 [kg/hr]	12

..

Table B.3: Variables with their correponding values as it is used for the simulation of biomass gasification.

Variables	**Value**	**Variables**	**Value**
STEAMGEN temperature [°C]	250	HEATER1 temperature [°C]	850
STEAM2 flow [kg/hr]	55	PREGASIF temperature [°C]	850
MOISTURE (at 105°C) flow [kg/hr]	11,61	ASHSEP ash fraction out	1
O2 (at 20°C) flow [kg/hr]	38,84	CHARSEP char fraction out	1
DRYBIO (at 105°C) flow [kg/hr]	100	COOLER temperature [°C]	40
CHAR (at 850°C) flow [kg/hr]	1,64	SEPA6 H_2S fraction out	0,99
		SEPA6 CO_2 fraction out	0,095

Table B.4: The experimental data of the wet gas composition (N_2 free) as it is given in Hannula et al. [9] and the modified data that the model will produce, the yield of $C_3 - C_5$ in the experiment has been represented by C_3H_8, C_6H_6 and C_10H_8 in the modified data.

The product wet gas compositions (%-vol)		
Species	Experiment	Modified (to be reproduced)
CO	0,124	0.123
CO_2	0,226	0.224
H_2	0,168	0.167
N_2	0	0.00189
CH_4	0,056	0.055
C_2H_2	0,0004	0.0003
C_2H_4	0,0142	0.0013
C_2H_6	0,0031	0.0013
$C_3 - C_5$	0,0003	0
NH_3	0	0
H_2O	0,418	0.416
C_3H_8		0.00017
C_6H_6		0.00186
C_10H_8		0.0023

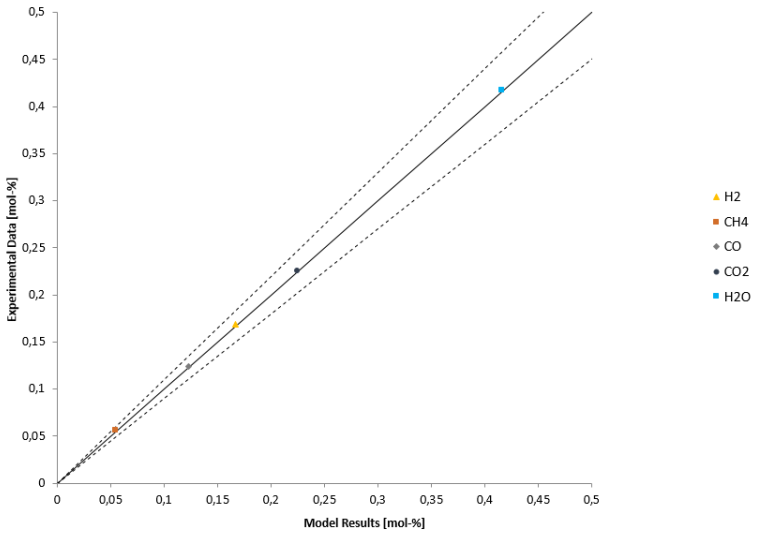

Figure B.1: Comparison between experimental and the model-produced gas compositions for the main gas components of the raw product gas. The two dotted lines enclose the region of 90% confidence around the linear line of slope 1.

Table B.5: Description of acronyms for components and streams of the gasification model.

Stream acronym	Description	Component acronym	Description
ASH	Ash of the biomass	ASHSEP	Ash separator
CHAR	The recycled char feed	CHARSEP	Char separator
CHAR2REC	Char of the gasification (to be recycled)	COOLER1	Cooler of the product gas
DRYBIO	Dry biomass feed	GASIFIER	The Gasifier
FEED0	The mix of feed material	HEATER1	Heater of the feed stream
FEED1	Heated feed material	MIXER1	Mixer of the input material
FEED2	Elementary components of the feed material	PREGASIF	Pre-gasifier (decompose the biomass into its elementaries)
H2S	Hydrogen sulfide	SEPA6	Separator of hydrogen sulfide
MOISTURE	Water in the biomass	STEAMGEN	The steam generator
O2	Oxygen		
STEAM1	Steam		
STEAM2	Steam		
SYNGAS0	The product of gasification (product gas+ash+char)		
SYNGAS1	The product gas and char		
SYNGAS2	The product gas		
SYNGAS3	The cooled product gas		
SYNGAS4	Th syngas (product gas without H_2S)		

Table B.6: Descriptions for streams and components of the methanation reactor.

Streams	Descriptions	Components	Descriptions
SYNGAS4	The product gas cleaned from H_2S	COLER2	Cools the product gas
SYNGAS5	The product gas cooled down to 40°C	SEP1	Dry the product gas, flash out the water
SYNGAS6	The dried product gas	COMP1	Multi-compressor, which has 6 stages
P-MET1	Pressurised product gas	$PUMP_i$ for i = 0,1...6	Pumps that pressurise the condansates
COND0	Water from the flash	MIXER2	Mix the pressurised gas and the water (MAKEUP1)
$COND_i$ for i = 1,2..5	Condansate from each stage of multi-compressor	MIXER3	Mixs the condansates from the pumps
$CONP_i$ for i = 1,2..5	Condansate from the pumps	SPLITTER	Splits the condansate
COND6	All the condansate from the pumps added together	HEATER2	Heats up the product gas and water
COND7	The remaining water flashed out of the reactor	RG_i for i = 1,2,34	RGIBBS reactor to uppgrade the methane content of the product gas
MAKEUP1	Water being supplied back to the product gas	$COOLER_i$ for i = 3,4,5,6	Cools the product gas down after reactors.
P-MET2	The mixture of water and the product gas (pressurised)	HO2REM1	Dryer
P-MET3	The heated up mixture of the product gas and water		
P-MET4	The product gas after the WSG reaction		
P-MET5, P-MET6 MET1, MET2, MET3 MET4, DRYING1	Streams of the product gas where CH_4 is succesively efter each reactor upgraded. The streams are inter-cooled between the reactors.		
CO2+CH4	The stream that contains mainly CH_4 and CO_2		
COND8	The water do be flashed out of the methanation reactor		

Table B.7: Variables and values for the operation parameters in the methanation process.

Variables	**Value**	**Variables**	**Value**
COOLER2 temperature (°C)	40	PUMPi dischrage pressure (bar) for i = 1,2...6	14
COOLER2 pressure drop (bar)	0	SPLITTER fraction for MAKEUP1	1
SEPA1 duty (W)	0	HEATER2 temperature (°C)	270
SEPA1 pressure drop (bar)	0	COOLERi pressure drop (bar) for i = 3,4,5	-1
COMP1 (isentropic) discharge pressure (bar)	14	COOLERi temperature (°C) for i = 3,4,5	200
COMP1 number of satges	6	COOLER6 temperature (°C)	40
Outlet temperature for stage 1 to 5 (°C)	80	COOLER6 pressure drop	0
Duty for the last stage (W)	0	HO2REM1 fraction for water removed	0,999
COMP1 pressure drop (bar)	0,005		

Table B.8: Properties of Biogas type A and B according to Swedish standard SS 15 54 38 [8].

Properties	Type A	Type B
Wobbeindex (MJ/m^3)	44,7 – 46,4	43,9 – 47,3
CH_4 content (vol-%)	97 ± 1	97 ± 2
Water content (mg/Nm^3)	32	32
O_2 content (max, vol-%)	1,0	1,0
$CO_2 + N_2 + O_2$ (vol-%)	4,0	5,0
Sulfur contaminants (mg/Nm^3)	23	23
NH_3 (mg/Nm^3)	20	20

C

Description of acronyms and their values in the Sabatier Process

Table C.1: The description of stream and component acronym in the simulation of Scenario 1 and 2.

Stream acronym	**Description**	**Component acronym**	**Description**
CO2+CH4	From methanation reactor, contains mainly CO_2 and CH_4	MIXER4	Mix the gas stream with recycled CO_2 and H_2
MET5	CO2+CH4 mixed with H_2 from electrolysis and the recycled CO_2	COMP2	Pressurize the gas stream
MET6	Pressurised stream of MET5	HEATER3	Heat up the gas stream
MET7	Heated stream of MET6	RP1	RPLUG where the Sabatier reaction occur
MET8	The stream rich in CH_4 after the Sabatier reactor	TUB1	The turbine to depressurize the stream
MET9	Pressurised stream of MET8	COOLER7	Cool down the gas
MET10	Cooled stream of MET9	H2OREM2	Dry the gas by removing water vapor
COND9	Condensed water out	CO2REM1 CO2REM2	Removes CO_2 off the gas
MET11	Dried gas, rich in CH_4	H2REM	Remove the hydrogen from the gas stream
CO2SEP, CO2SEP1 CO2SEP2	CO_2 removed from the gas stream.	CO2MIX	Mix the removed CO_2
MET12 MET13	Stream with the majority of CO_2 removed	CO2SPLIT	Split the stream of CO2

Table C.2: Continuation of Table C.1.

Stream acronym	**Description**
CO2OUT	The stream of CO_2 removed from the gas stream
CO2TOT	The stream of CO_2 removed out
CO2REC	CO_2 recycled
H2	Hydrogen supplying stream
BIOMETHA	Stream of biomethane to the grid
H2REC	Stream of recovered H_2

Table C.3: The description of acronyms for streams and components in the simulation of Scenario 3 and 4.

Stream acronym	**Description**	**Component acronym**	**Description**
CO2+CH4	The gas stream that contain mainly CO_2 and CH_4	CO2REM1 CO2REM2	The separators of CO_2
1STCO2R	Stream with 92% CO_2 removed	CO2MIX	Mixer ofCO_2 streams
CO2SEP1 CO2SEP2	Streams of pure CO_2 to the Sabatier	COMP2	Compressor
MET8	Pressurized stream of CO_2	CO2SPLIT	Valve to release certain amount of CO_2
CO2OUT	Certain amount of CO_2 removed through valve	MIXER4	Mixer of H_2 and CO_2
SAB1	The remaining CO_2 to the Sabatier	HEATER3	Heater
SAB2	Mixture of H_2 and CO_2	RP1	RPLUG reactor for the Sabatier process
SAB3	The heated stream of SAB2	TURB1	Turbine to depressurize the gas stream
SAB4	The product of Sabatier process	COOLER7	Cooler of the gas stream SAB5
SAB5	Depressurized stream	H2OREM2	Dryer
SAB6	The cooled gas stream	H2REM	Separates H_2 from the gas stream
SAB7	The dried gas stream	PRODMIX	Mixer of the gas streams
H2REC	The recoveredH_2		
PRODGAS1 and PRODGAS2	The stream of biomethane from methabation and Sabatier reactor, respectively		
BIOMETHA	The stream of biomethane ready to be injected into the grid		

Table C.4: Variables with their respective values for the simulation of Sabatier process in all the Scenarios.

Variable	**Value**	**Variable**	**Value**
CO2+CH4 flow [kg/hr]	137,2	TURB1 discharge pressure (bar)	10
H2 flow [kg/hr]	Variable	TURB1 isentropic efficiency	0,88
COMP2 discharge pressure (bar)	60	COOLER7 temperature [°C]	40
COMP2 isentropic effeciency	0,88	H2OREM2 water fraction removed	0,999
HEATER3 temperature [°C]	340	CO2REM CO_2 removed	0
RP1 length [mm]	1000	H2REM H_2 removed (scenario 1)	0
RP1 diameter [mm]	30	H2REM H_2 removed (scenario 2)	0,9
Catalyst loading [kg]	36	CO2REM1 and CO2REM2 fraction of CO_2 removed	0,9
Catalyst particle density [kg/m^3]	1700		

D

Calculation of economic performance and description of the acronym used

Operational profits (as revenues-costs) are calculated in equation D.1-D.16. Descriptions about the dependent and independent variables of those equations are presented in Table D.1 and Table D.3.

Assumptions. The electricity cost for industries is 0,048$/kWh in Sweden [65]. Electricty from the intermittent source are assumed to be produced at the off-peak period with the price 50% that of the given one. The price of the biogas type-A is considered to be that of the price which the consumer pay at the refueling station, $1,98/kg [66]. Price for the type-B is calculated based on type-A according to type-A/type-B = 0,144/0,109 ([67]).

D.1 Costs

For the dryer, the only considered costs are electricity consumed in the fans. The required heat in the belt dryer was provided by the internally recovered heat of the gasification process.

$$DFAN = C_{el} * (PFAN1 + PFAN2) \tag{D.1}$$

For the gasification of the biomass:

$$GO2 = C_{O2} * \dot{m}_{O2} \tag{D.2}$$

$$GBIO = C_{BIO} * LHV_{biomass} * \dot{m}_{BIOMASS} \tag{D.3}$$

$$\begin{aligned} GH2S = C_{MDEA} * MAKEUP1 * \dot{m}_{H_2S} + \\ (0,85/0,15) * MAKEUP1 * C_{water} * \dot{m}_{H_2S} \end{aligned} \tag{D.4}$$

For the methanation reactor:

$$MMCOMP = C_{el} * M_{power} \tag{D.5}$$

$$MCAT = C_{catalyst} * MR_{consum} \tag{D.6}$$

MR_{consum} is calculated by retrieving the catalyst load from the simulation and assuming the regenration time of the catalyst to be 1000 hr[42].
For the Sabatier reactor:

$$SH2 = \dot{m}_{H_2} * H_{el} * C_{el} \tag{D.7}$$

$$SCOMP_{60bar} = C_{el} * S1_{power} \tag{D.8}$$

$$SCAT = C_{catalyst} * MR_{consum} \tag{D.9}$$

$$H2_{remove} = \dot{m}_{H_2} * \frac{\rho_{silica} * V_{PSA}}{1000 * \dot{m}_{PSA}} * C_{catalyst} + \dot{m}_{H_2} * E_{H2} \tag{D.10}$$

$$\begin{aligned} CO2_{remove} = C_{MEA} * MAKEUP2 * \dot{m}_{CO_2} + \\ (0,7/0,3) * MAKEUP2 * C_{water} * \dot{m}_{CO_2} \end{aligned} \tag{D.11}$$

$$COMP_{30bar} = C_{el} * S2_{power} \tag{D.12}$$

D.2 Revenues

Revenues are generated by selling SNG, steam (at 400K), electricity and the byproduct oxygen of the electrolysis, which are estimated, respectively, according to the following equations.

$$R_{SNG} = \dot{m}_{SNG} * C_{SNG} \tag{D.13}$$

$$R_{steam,400} = C_{steam,400}/h_{steam,400} * P_{steam,400K} \tag{D.14}$$

$$R_{el} = C_{el} * NET_{el} \tag{D.15}$$

$$O_{2,byproduct} = C_{O2} * \dot{m}_{O2,byproduct} \tag{D.16}$$

$\dot{m}_{O2,byproduct}$ is calculated from reaction 2.15, and varies with the amount of H_2 produced for the Sabatier reaction; note that only the net hydrogen supplied is considered in those cases where H_2 is separated (and recycled).

Table D.1: Independent variables and their values to calculate operational costs. "Retrieved" corresponds to the values which are taken from the simulation.

Variable	**Value**
C_{el} (electricity price) [$/kWh]	0,024 [65]
C_{SNG} (cost of biogas A) [$/kg]	1,98 [66]
C_{SNG} (cost of biogas B) [$/kg]	1,5 [66]
$\dot{m}_{BIOMASS}$ (massflow of dry biomass) [kg/hr]	100
$\dot{m}_{CO_2}$ (massflow of CO_2 removed) [kg/hr]	Retrieved
$\dot{m}_{H_2}$ (massflow the injected hydrogen) [kg/hr]	variable
$\dot{m}_{H_2S}$ (massflow of H_2S removed) [kg/hr]	Retrieved
$\dot{m}_{O2}$ (massflow of oxygen) [kg/hr]	Retrieved
$\dot{m}_{SNG}$ (massflow of the biogas)	Retrieved
0,7/0,3 (the weight fraction between water and MEA)	
0,85/0,15 (the weight fraction of the water and MDEA)	
C_{BIO} (cost of biomass) [$/MWh]	20,92 [68]
$C_{catalyst}$ (cost of the catalyst, Nickel) [$/kg]	1,0-10 [42]
C_{MDEA} (cost of MDEA) [$/kg]	2,43 [42]
C_{MEA} (cost of MEA) [$/kg]	1,92 [42]
C_{O2}(oxygen cost) [$/kg]	0,16-0,20 [42]
$C_{steam,400}$ (cost of a steam at 400K) [$/ton]	20 [42]
C_{water} (cost of the water for the solution) [$/ton]	0,5 [42]
H_{el} (electric consumption for producing H_2) [kWh/kg]	Electrolysers
$h_{steam,400}$(specific enthalpy of evaporation at 400K) [kJ/kg}	2183,06
$LHV_{biomass}$ [kJ/kg]	18,716 [10]
M_{power} (electric power to the multi-compressor [kW]	Retrieved
MAKEUP1 (the MDEA loss during operation) [kgMDEA/tonH_2S]	0,3-0,8
MAKEUP2 (MEA loss during the operation) [kgMEA/kgCO2]	0,3-0,8 [42]
MR_{consum} (catalyst consumption in methanation) [kg/hr]	Calculated
NET_{el}(net electricity produced)	Retrieved
$P_{steam,400K}$ available power at 400K, from GCC)	Retrieved
PFAN1 (power of,FAN1) [kW]	Retrieved
PFAN2 (power of,FAN2) [kW]	Retrieved
$S1_{power}$ (electric power for compressor to 60 bar) [kW]	Retrieve

Table D.2: Continuation of Table D.1

Variable	**Value**
ρ_{silica} (density of the silica gel) [g/cm^3]	1,15 [43]
C_{O2} (prise of oxygen) [$/kg]	0,16-0,20 [42]
E_{H2} (electric energy consumption in PSA) [kWh/kgH2]]	0,53 [43]
$\dot{m}_{O2,byproduct}$ (oxygen mass flow) [kg/hr]	Retrieved
m_{PSA} (Hydrogen mass flow in PSA operation of [43] [kg/hr]	134,1[43]
S_{power} (electric power to compressor to 30 bar) [kW]	Retrieved
V_{PSA} (volume of the chamber in PSA operation [43]) [m^3]	1,374 [43]

Table D.3: Descriptions of the dependent variables to calculate the operational costs

Variable	Descriptions
DFAN	Costs due to the operation fans in the dryer
GO2	Cost to buy the biomass
GH2S	Costs to remove H_2S
MMCOMP	Costs to operate multicompressor in the gasification
MCAT	Costs due to catalyst consumption in the methanation reactor
SH2	Costs to buy H_2 from electrolysers
$SCOMP_{60bar}$	Costs to compress the gas to 60 bar in the Sabatier reactor
SCAT	Costs due to catalyst consumption in the Sabatier reactor
$H2_{remove}$	Costs to remove H_2
$CO2_{remove}$	Costs to remove CO_2
$COMP_{30bar}$	Costs to operate the compressor to pressurize the gas to 30 bar
R_{SNG}	Revenues from selling biomethane
$R_{steam,400}$	Revenues from selling the steam at 400K
R_{el}	Revenues generated from selling the net electricity produced
$O_{2,byproduct}$	Revenues generated from selling the byproduct oxygen

Table D.4: Independent variables and their values used in the calculation of thermodynamic performance indicators. "Retrieved" means the value is gotten from the simulations.

Variable	Value
LHV_{CH_4} [MJ/kg]	50.00 [69]
LHV_{H2} [MJ/kg]	119.96 [69]
$\dot{m}_{biomass}$(massflow of dry biomass)[kg/hr]	100
$\dot{m}_{CH_4}$ (massflow of methane) [kg/hr]	Retrieved
$\dot{m}_{H2,f}$ (massflow of H_2 in the feed) [kg/hr]	Variable
$\dot{m}_{H2,b}$ (massflow of H_2 in the biogas) [kg/hr]	Retrieved
$\dot{m}_{CO_2}$ (massflow of CO_2 scrubbed) [kg/hr]	Retrieved
$\dot{m}_{H_2S}$ (massflow of H_2S scrubbed) [kg/hr]	Retrieved
E_{CO_2} (energy required to absorb CO_2 [MJ/kg]	3,3 [41]
E_{H_2S} (energy required to absorb H_2S) [MJ/kg]	5,23 [1]

E

Model sensitivity and biogas compositions

The most common application of P2G technology in the gasification process is to provide H_2, by electrolysis, which could be used for the adjustment of H_2/CO ratio of the syngas prior to methanation or in the production of biomethane in the Sabatier process. Even though it is not prevalent, the other application of P2G in the gasification is the introduction of electricity as a form of heat in the gasifier. Alamia [7] discusses that resistance heater in a gasifier can provide the heat energy which would otherwise has to be internally provided by the combustion of the char. This would decrease char combustion and increase char gasification.

Investigating the effect of external heat supply on the gasifier was in our interest at the early stage of the project. However, it has been found out that the developed gasifier (PREGASIF and GASIFIER reactors) happened to be insensitive to external heat supply, meaning that the composition of the product gas remain unchanged with external heat supply. It was due to the fact that RStoic reactor does not take the effect of thermodynamic properties (temperature and pressure) on the given reaction into consideration. We tried to evaluate the effect of external heat supply by reducing the combustion reaction of char (reaction 2.1) with the amount of the external heat energy to be supplied. Here again, it was not evident which of the endothermic reactions of the char gasification are favoured by this action. The correct evaluation for the effect of external heat supply could be done by separating the gasification process into different steps (pyrolysis and char combustion) and using reactors such as RGibbs, REquil and RPlug which calculates phase and chemical equilibrium as a function of thermodynamic properties. If RStoic has to be used, scientific investigations about the favoured endothermic reactions have to be done.

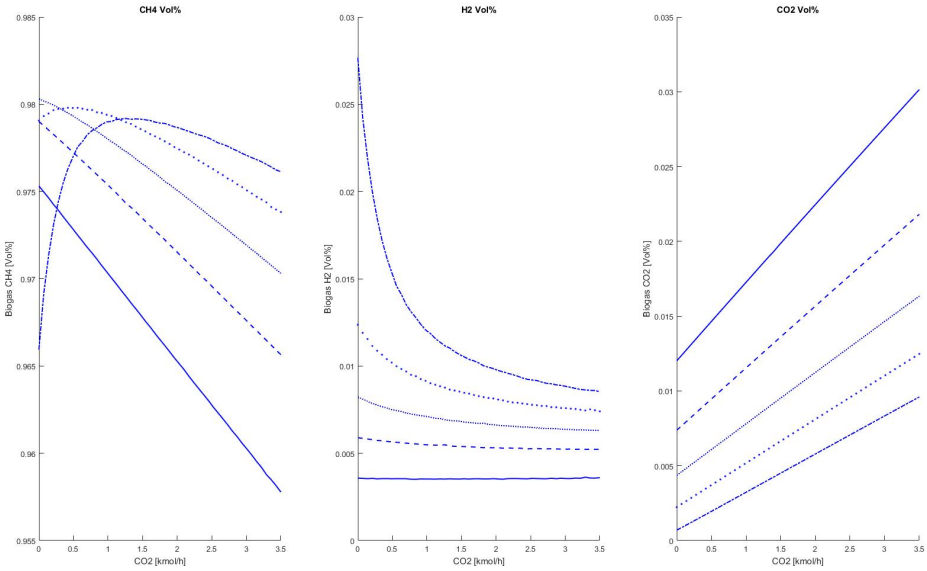

Figure E.1: The variation of biogas composition as H_2 and CO_2 varies in Scenario 1.

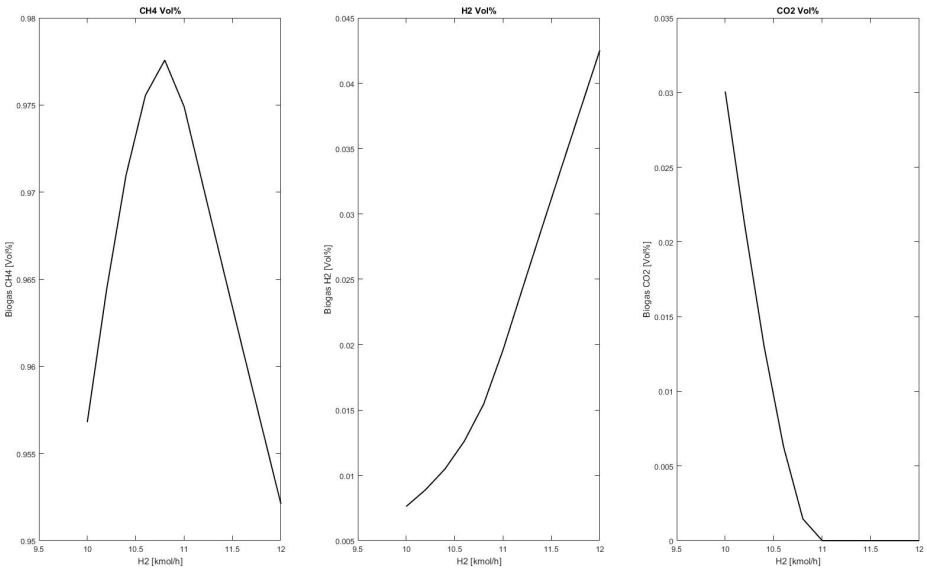

Figure E.2: The ASPENPLUS model for the simulation of scenario 4. Descriptions to the acronym of streams and components are given in Table C.3 in Appendix C

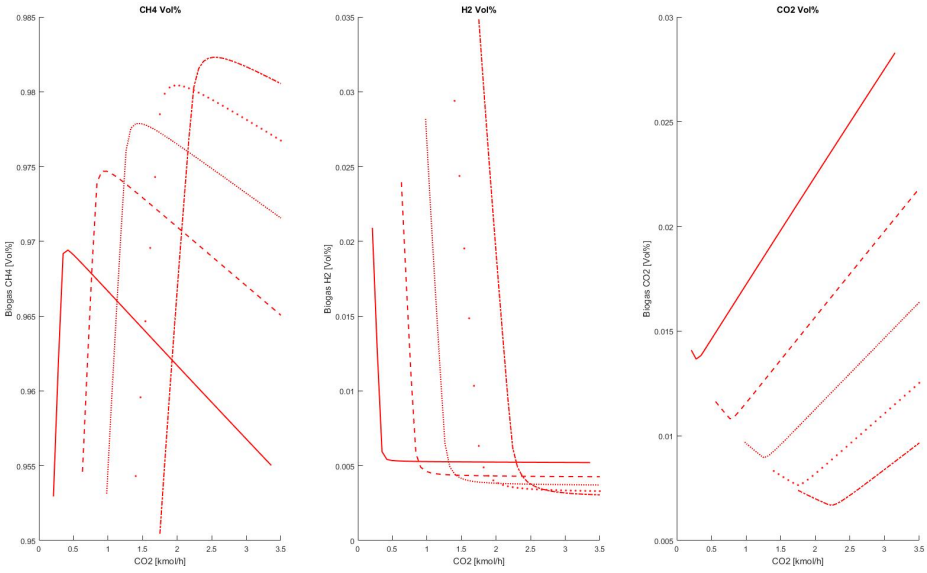

Figure E.3: The variation of biogas composition as H_2 and CO_2 varies in Scenario 3.

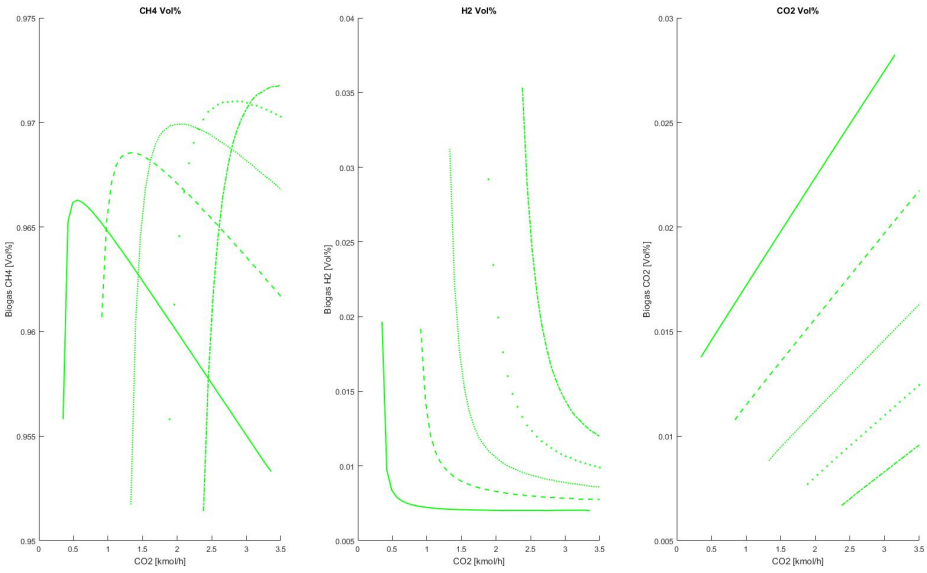

Figure E.4: The variation of biogas composition as H_2 and CO_2 varies in Scenario 4.